# Target Motion Analysis of a Source in a Constant Turn from a Nonmaneuvering Observer

Julien Clavard, Denis Pillon, Annie-Claude Pignol, Claude Jauffret

# Target motion analysis of a source in a constant turn from a non-maneuvering observer

**Julien Clavard, Denis Pillon**

Thales Underwater Systems

525 Route des Dolines

06903 Sophia-Antipolis, France

julien.clavard@fr.thalesgroup.com

denis.pillon@fr.thalesgroup.com

**Annie-Claude Pignol, Claude Jauffret**

Université Sud Toulon-Var

CNRS, IM2NP (UMR 6242)

Bâtiment X, BP 132, 83957

La Garde Cedex, France

pignol@univ-tln.fr, jauffret@univ-tln.fr

**Abstract:**

**The passive target motion analysis (TMA) of a source in constant turn motion by a platform moving with a constant velocity vector is addressed in this paper. The observer acquires either bearing measurements or bearing and frequency measurements. Firstly the bearings-only TMA is investigated. The observability conditions are established and the performance is analyzed with the Cramér-Rao lower bound. The behavior of the maximum likelihood estimator is evaluated using Monte-Carlo simulations, for various typical scenarios. The bearings and frequencies TMA is subsequently analyzed in the same way. Its performance is compared with that of the bearings-only TMA to evaluate the improvement**

**brought about by frequency measurements, in some typical scenarios. Tactical aspects are also investigated.**

**Keywords:** Constant turn motion, bearings-only target motion analysis, bearings and frequencies target motion analysis, passive tracking, maximum likelihood estimate, Cramér-Rao lower bound.

# I Introduction

In TMA, when a sole passive sensor is employed, just few kinematic models have been adopted, compared to numerous models encountered in the active tracking domain (see [1] and its references). This is one of the consequences of the poor quality of the information contained in the data (implying a lack of observability) acquired by a passive system which does not directly measure the position of a source, unlike an active sensor.

The polynomial kinematic models are most often used; the oldest (and simplest) is the constant velocity motion or CV motion (see [2] to [5]). The higher order is also exploited (see [6] to [8]).

Indeed, in the classic bearings-only TMA (or BO-TMA), it has been proved that the observer must have a model of higher order to the source's motion model to get observability but it is not sufficient ([7] [8]).

Several authors have proposed more sophisticated kinematics derived from this basic deterministic model, for instance, a segmented trajectory with unknown duration of each leg ([10] [11]). In [12], we proved the interest of this model when the target's speed is constant: in this case, the observability is obtained without maneuver of the observer (except in some pathological geometry).

But these models are too restrictive. One of the challenges of the passive TMA is to construct a realistic model for which observability is acquired when the observer does not maneuver. We propose here to consider a target kinematic model for which the maneuver is not instantaneous: the legs of unknown duration are linked by arcs of a circle at constant speed (as in [13] [14]).

The key model being the constant turn motion (CT motion), we will start by analyzing it. From our knowledge, this deterministic model and its use in BO-TMA has never yet been employed. Surprisingly, the first mathematicians to have treated a very similar problem are the French Pierre-Simon de Laplace [16] in

1780 and the German Karl Friedrich Gauss [17] in 1795. They identified the parameters of the elliptical orbit of an asteroid from angular measurements of lines of sight given by a telescope. They proved that with three angles collected at different times, they were able to recover the whole trajectory of the asteroid. Thus they introduced for the first time the notion of discrete observability in a TMA problem. At this time, Gauss invented the method of least squares [18]. This method is already used for satellite orbit determination by ground based telescope [19]. Recently, a Chinese team proposed a 3D TMA method that is very similar [20][21]. Indeed, they collect angular measurements from a High Earth Orbit (HEO) satellite in order to localize a Low Earth Orbit (LEO) satellite. The trajectory of the observer is elliptical whereas that of the source is a circle whose center is known (the center of the Earth).

Nevertheless, the nature of these aerospace problems is different from the one considered in this paper: Here, the rotation center is unknown; as a consequence, the observability is not *a priori* established. This kind of kinematic is still quite common:

- Sources like lightweight torpedoes in underwater environments and drones in aerial environments, for example, travel along an arc of a circle,
- Observers manoeuver in an arc of a circle to get observability in BO-TMA [3] [11] [14].

More generally, a surface ship or a submarine follows an approximately circular motion when it changes its heading.

The problem treated here is hence the BO-TMA of a source whose trajectory is composed of a succession of legs and arcs of a circle, its speed being constant whereas the duration of each segment is unknown.

Let us recall that in the classic case (target and observer with constant velocity vector), an additional frequency track alleviates the problem of observability ([8] [9]). Moreover, the greater the number of frequencies, the more accurate the result will be [23].

It is legitimate to ask the same question when the source is in CT motion.
The computation of the Cramér Rao lower bound (CRLB) together with Monte Carlo simulations will allow us to evaluate the performance of proposed estimates in a set of realistic scenarios.
The underlying system is twice nonlinear: the state equation is nonlinear (due to the CT motion) as well as the measurement equation. Consequently, we can no longer use the technique that consists of transforming the natural system into an equivalent linear system (as in [8]). We have been constrained to use an original mechanism based upon strong tools of analysis mathematics.

The basic questions posed here are:

- Does the observer have to maneuver to get a unique solution if only bearings are available?
- Would it be helpful to take into account a frequency measurement?

- What are the consequences tactically speaking?

We propose to answer these questions more completely than in [15].

This paper is organized in five main sections, followed by the conclusion and an appendix.

In section II, after having defined the assumptions and the notations, we analyze the observability when the observer measures angles only.

Section III is devoted to the presentation of the maximum likelihood estimator (MLE) and its performance. The numerical aspect is discussed.

In section IV, we deal with the same problem when additional frequency measurements or track(s) are available: observability, the MLE and its performance are analyzed.

Section V establishes the tactical advantages between a maneuvering and a non-maneuvering platform in terms of accuracy of their respective TMA, when only bearings are available and when bearings and frequencies are.

A conclusion ends the paper.

The appendix is devoted to the development of the observability analysis.

# II The Bearings-only constant turn TMA (BO-CTTMA)

## II.1 Assumptions and notations

We consider an observer O and a source (or target) S moving in the same plane. We assume that at any time, the location of the source is different from the location of the observer (collision is impossible).

The source is traveling along an arc of a circle at constant speed (say constant turn or CT motion); meanwhile the observer follows a constant velocity (CV motion). All the angles are referenced clockwise, from North as in any usual TMA problem.

At time $t \in [0, T]$, the source's position is given by

$$P_S(t) = \begin{bmatrix} x_S(t) \\ y_S(t) \end{bmatrix} = \begin{bmatrix} x_C \\ y_C \end{bmatrix} + \rho_C \begin{bmatrix} \sin(\omega t + \varphi) \\ \cos(\omega t + \varphi) \end{bmatrix}$$

where

- $P_C = [x_C \quad y_C]^T$ is the location of the center of the circle,
- $\rho_C$ is the radius of this circle.
- $\omega \neq 0$ is the constant turn rate, positive if the motion of the target is clockwise,
- $\varphi$ is the "initial angle" (relative to North), when the source starts its motion.

Note that the speed of the source denoted $v_S$ is linked to the turn rate and the radius of the circle by $v_S = |\omega| \rho_C$.

The position of the observer at any time $t \in [0, T]$ is

$$P_O(t) = \begin{bmatrix} x_O(t) \\ y_O(t) \end{bmatrix} = \begin{bmatrix} x_O(0) + t\,\dot{x}_O \\ y_O(0) + t\,\dot{y}_O \end{bmatrix}$$

where $[\dot{x}_O \quad \dot{y}_O]^T$ is its constant velocity vector.

The noise-free bearing at time $t$ is given by $\theta(t) = \tan^{-1}\left[\dfrac{x_S(t) - x_O(t)}{y_S(t) - y_O(t)}\right]$.

The noise-free range between the source and the observer at time $t$ is denoted $R(t)$.

All these notations are illustrated in Fig. 1.

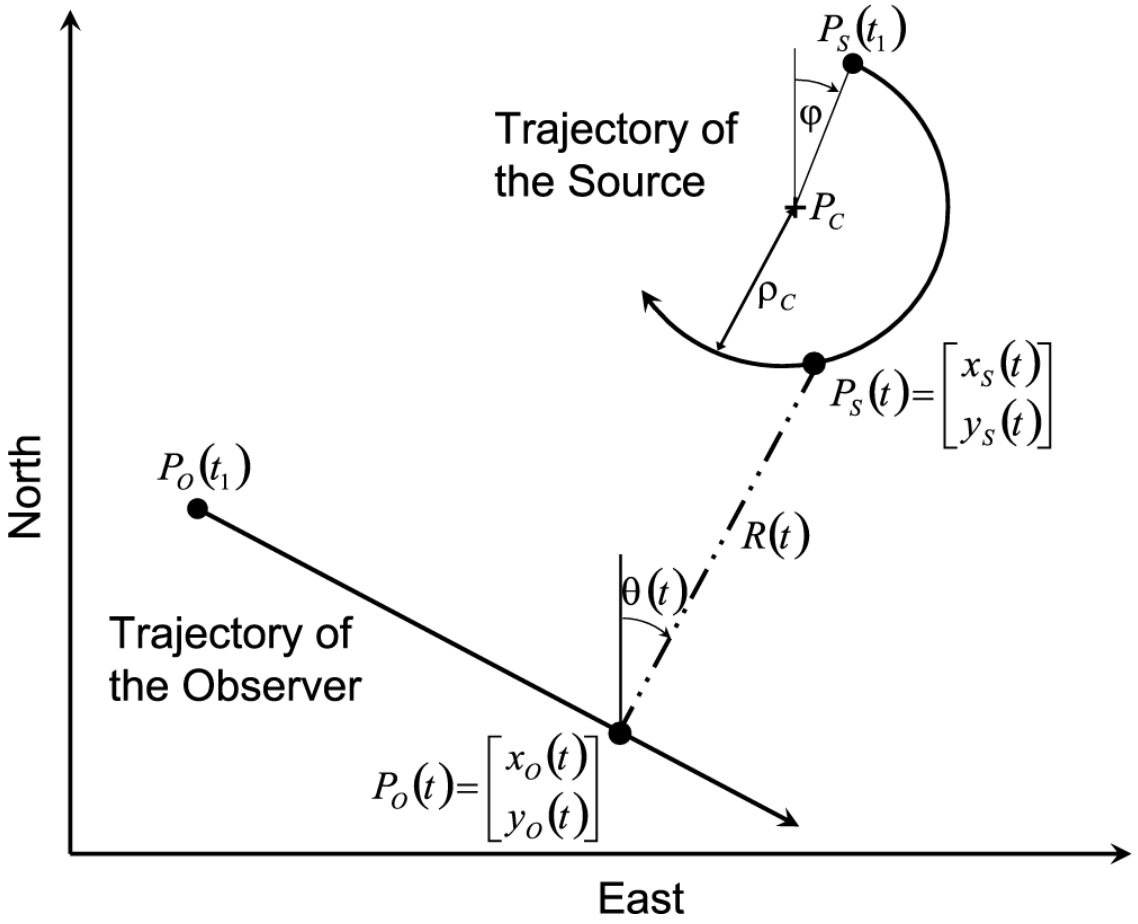


Fig. 1. Observer and source geometry of BO-CTTMA.

The trajectory of the source is entirely defined by the state vector $Z=\begin{bmatrix} x_C & y_C & \rho_c & \varphi & \omega \end{bmatrix}^T$.

To indicate that the bearings $\theta(t)$ are a function of the state vector, we will also employ the notation $\theta(Z,t)$.

At time $t_k$, the observer collects the measured bearings $\theta_m(t_k)$

$$\theta_m(t_k) = \theta(Z, t_k) + \varepsilon_\theta(t_k), \text{ for } k = 1, 2, ..., N \qquad (1)$$

where $\varepsilon_\theta(t_k)$ is the additive noise assumed to be zero-mean and Gaussian. Its covariance matrix is equal to $diag\left(\sigma_\theta^2(t_k)\right)$ (assumed to be known).

Note that the duration of any scenario is equal to $t_N$.

The aim of the BO-CTTMA is to estimate the state vector $Z$ from $\theta_m = \{\theta_m(t_1), \theta_m(t_2), \cdots, \theta_m(t_N)\}$.

## II.2 Observability analysis

In this section, three strong results about observability in continuous time are given. The proofs of the results are detailed in the Appendix.

### *II.2.a Source in CT motion*

RESULT 1 (*observability case):*

*The trajectory of any source in CT motion is observable from bearings-only measurements* $\theta(t)$ *for* $t \in [0, T]$ *if and only if the observer in CV motion is not motionless.*

RESULT 2 (*ambiguous trajectories in non-observability case):*

*If the observer is motionless and located at* $[x_O \quad y_O]^T$*, the trajectories of the sources detected on the same bearings as the source of interest are*

*homothetic. More precisely, if* $Z = \begin{bmatrix} x_C & y_C & \rho_c & \varphi & \omega \end{bmatrix}^T$ *is the state vector defining the trajectory of the source of interest, then any other homothetic trajectory is defined by*

$Z' = \begin{bmatrix} \mu(x_C - x_O) + x_O & \mu(y_C - y_O) + y_O & \mu\rho_c & \varphi & \omega \end{bmatrix}^T$, $\mu$ $(>0)$ *being the homothetic ratio.*

*If the observer is located in the circle in which the source is travelling, this set of trajectories is augmented with the trajectories defined as the intersection of the angular sector* $[\theta(0), \theta(T)]$ *and similar*[1] *circles, the rotation center of the similarity being at* $\begin{bmatrix} x_O & y_O \end{bmatrix}^T$*. The turn rate of these sources is the same.*

The first part of this result allows us to construct easily a $\mu$-homothetic solution:

The center of the circle $P_{C'}$ of the $\mu$-homothetic solution is given by $\overrightarrow{P_O P_{C'}} = \mu \overrightarrow{P_O P_C}$ and its radius is $\rho_{C'} = \mu \rho_C$. The lines of sight are the same.

Fig. 2 illustrates the case where the observer is outside the circle, whereas Fig. 3 gives an example when the observer is inside the circle. In both examples, the homothetic ratio $\mu$ is equal to 3.

[1] A similarity is obtained by composing of a rotation of angle $\psi$ and an homothety of ratio $\mu$.

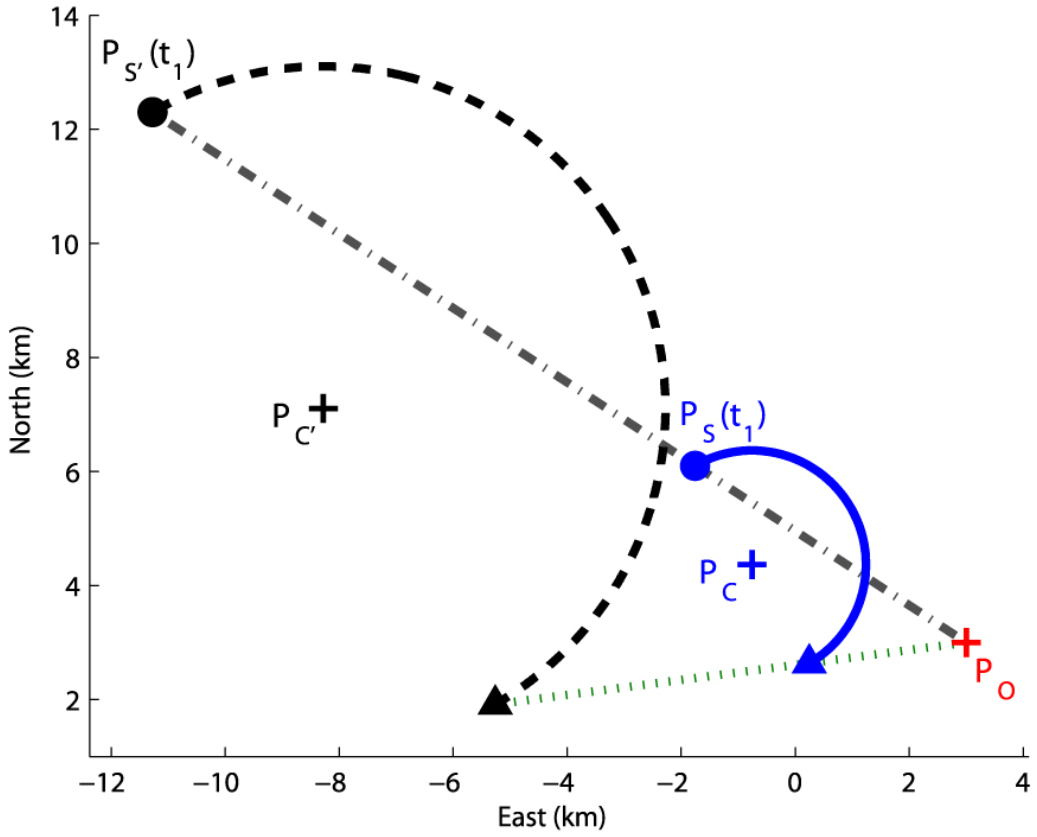


Fig. 2. Examples of homothetic trajectories: motionless observer outside the trajectory of the sources.

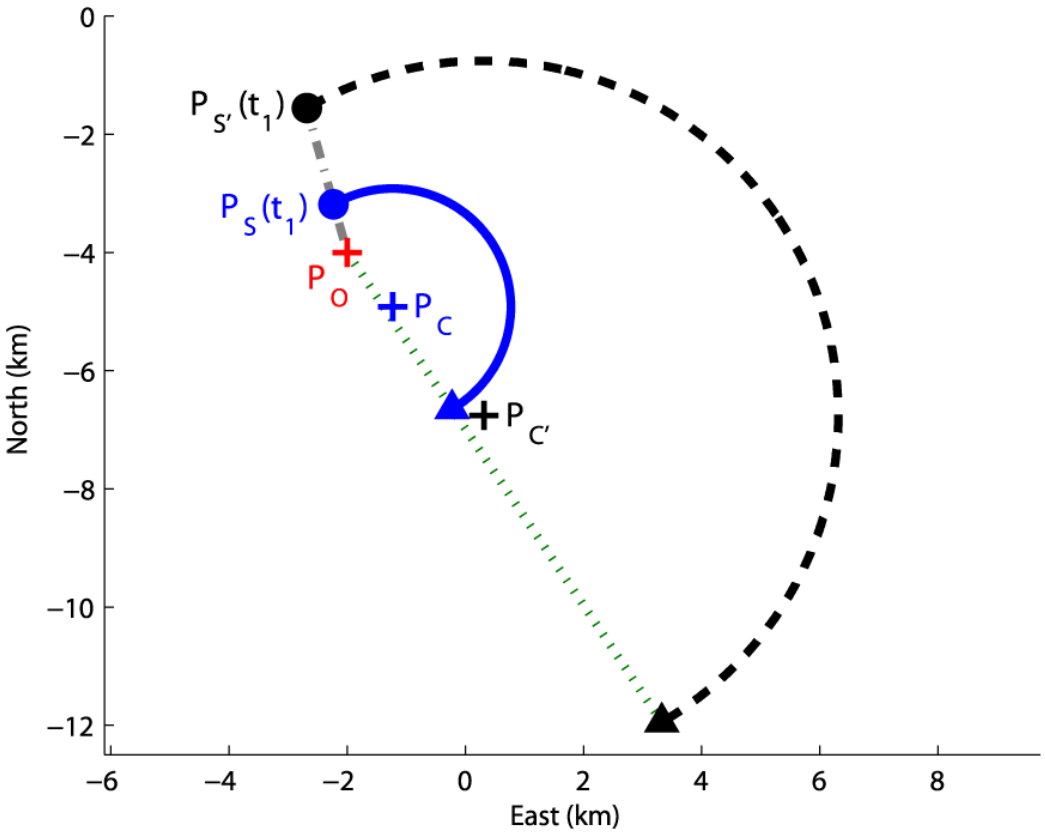


Fig. 3. Example of homothetic trajectories: motionless observer inside the trajectory of the sources.

In the second part of this result, the rotation angle $\psi$ is submitted to the following constraints (in order to insure that the intersection between the angular sector and the similar circle is not empty):

- If $\omega > 0$, then $\theta(T) - \theta_C - \frac{\pi}{2} < \psi < \theta(0) - \theta_C + \frac{\pi}{2}$,
- *If* $\omega < 0$, *then* $\theta(0) - \theta_C - \frac{\pi}{2} < \psi < \theta(T) - \theta_C + \frac{\pi}{2}$ .

Remarks:

From the above analysis, when the observer is motionless,

- knowledge of one parameter (the speed, the center of the circle, its radius) confers observability,
- the turn rate $\omega$ is observable,
- if the observer is not in the circle in which the source is moving, the initial angle $\varphi$ is observable too,
- the observer is located in this circle if and only if $\theta(t)$ is affine, *i.e.* $\theta(t) = at + b$; in this case, $a = \frac{\omega}{2}$ and $b = \frac{\varphi + \theta_C}{2}$, where $\theta_C$ is the azimuth of the center $P_C$ of the circle.

### *II.2.b Distinguishability between a source in CV motion from an another in CT motion*

In this subsection, we use a notion derived from observability called distinguishability, corresponding to the following problem:

Suppose that the source of interest $S$ is in CT motion. We need to determine if another source, denoted $S'$, in CV motion, could be detected with the same bearings as $S$. The answer is given by the following property.

RESULT 3 (*distinguishablity of motion models in continuous time*)

*Consider an observer in CV motion and the source of interest $S$ in CT motion.*

*Then there is no source in CV motion detected with the same bearings* $\theta(t)$ *for* $t \in [0, T]$*. The CT motion is said to be distinguishable from the CV motion by bearings only.*

Remark:

- If the observer is not motionless, observability is ensured only for the source in CT motion.
- Otherwise, the two sources are unobservable.

### *II.2.c Observability of segmented trajectories (succession of legs and arcs of a circle at constant speed)*

The previous results allow us to get a very general and important result about observability when the observer is in CV motion, with a non-zero speed.

Now, suppose that during $[0, \tau]$, the source of interest $S$ is in CV motion, and during $[\tau, T]$, it is in CT motion. The maneuver time $\tau$ is unknown.

Consider another source, say $S'$, which is in CV motion during $[0, \tau']$, and in CT motion during $[\tau', T]$.

- If $\tau = \tau'$, then during $[\tau, T]$, $S$ and $S'$ are in CT motion. From Result 1, the two sources are identical.
- If $\tau \neq \tau'$, for instance $\tau < \tau'$, then during $[\tau, \tau']$ $S$ is in CV motion, while $S'$ is in CT motion. This is incompatible with RESULT 3.

By extension, we obtain the following and principal result:

RESULT 4

> *Consider an observer in CV motion collecting bearings-only measurements* $\theta(t)$ *for* $t \in [0, T]$*. Suppose now that the source of interest has a constant speed during the scenario. If its trajectory is composed of a succession of segments (a segment being a kind of motion – CT or CV -), if there is at least one segment in CT motion, then the entire trajectory is observable.*

Note that if the observer is motionless and located at $P_O$, then the trajectory of the source is unobservable since any homothetic trajectory (by the homothety whose center is $P_O$ and the ratio is $\mu$) would be detected in the same bearings.

We illustrate this result using the example drawn from [12]: a source whose trajectory is composed of two legs with a constant speed is proven to be observable if and only if $(V_2 - V_1)^T V_O \neq 0$, where $V_i$ is the velocity of the source during the $i^{th}$ leg and $V_O$ is the velocity of the observer. If the two legs are linked with an arc of a circle, this condition vanishes: an illustration of this result is given in Fig. 4. An example of estimation for such a trajectory can be found in [12].

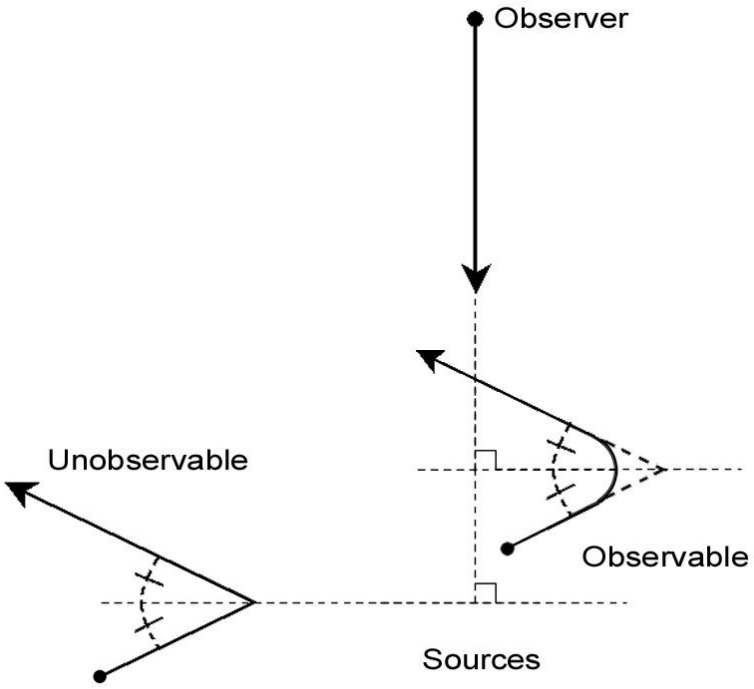


Fig. 4. Unobservable and observable trajectories.

# III Maximum likelihood estimator in BO-CTTMA

## III.1 Algorithmic aspect

The noise being assumed to be Gaussian, the MLE is identical to the least squares estimator. So the criterion to minimize is

$$C(Z) = \sum_{k=1}^{N} \frac{1}{\sigma_\theta^2(t_k)} \left[\theta_m(t_k) - \theta(Z, t_k)\right]^2 .$$

The minimization is done in three steps:

- initialization by a choosing an initial point in a coarse grid,
- ten iterations of the Gauss-Newton routine,

- then as many iterations as necessary of the Newton-Raphson routine up to convergence (declared when the routine can no longer minimize the criterion) [28].

However, the risk of stalling in a local minimum exists; so, the returned estimate $\hat{Z}$ is subjected to an acceptation test by comparing $C(\hat{Z})$ to a threshold. The threshold is computed assuming that $C(\hat{Z})$ is approximately Chi-square distributed with $N-5$ degrees of freedom, hence approximately Gaussian distributed $G(N-5, 2N-10)$. The estimate $\hat{Z}$ is accepted if $C(\hat{Z})$ is less than $N-5+3\sqrt{2N-10}$ (99.5% of the population). Then we compute the corresponding $\hat{Z}_N$ (which contains the final position).

The performance of the MLE must be compared to the Cramér-Rao lower bound (CRLB) in order to make a conclusion about its behavior. This motivates the next section (III.2) in which we compute the Fisher information matrix (FIM).

As in any problem of TMA, giving a general formula of the performance of the MLE is very difficult: the problem is highly nonlinear and depends strongly on the scenario. To overcome this, we have recourse to Monte Carlo simulations, run on a set of typical scenarios. Firstly, we focus our study on the accuracy of the estimated final range. Secondly, we evaluate the accuracy of each component of the state vector.

### III.2 Computations of the FIM and the CRLB in the BO-CTTMA

Under the previous assumptions given in II.1, the FIM is given by the following classic formula

$$F\left(Z|\theta_m\right)=\sum_{k=1}^{N}\frac{1}{\sigma_\theta^2\left(t_k\right)}\nabla_Z\theta(Z,t_k)\nabla_Z^T\theta(Z,t_k)$$

where $\nabla_Z\theta(Z,t_k)$ is the gradient of the measurement model w.r.t. the state vector.

In practice, the position of the source at time $t_N$ (the final time) is of great interest. So we compute the FIM, relative to $Z_N=\left[x_S\left(t_N\right)\quad y_S\left(t_N\right)\quad \rho_C\quad \varphi\quad \omega\right]^T$. Note that only its first two components are different.

$$F\left(Z_N|\theta_m\right)=J_{Z,Z_N}^T F\left(Z|\theta_m\right)J_{Z,Z_N}$$

where $J_{Z,Z_N}=\begin{bmatrix}1 & 0 & -\sin(\omega\, t_N+\varphi) & -\rho_C\cos(\omega\, t_N+\varphi) & -t_n\rho_C\cos(\omega\, t_N+\varphi)\\ 0 & 1 & -\cos(\omega\, t_N+\varphi) & \rho_C\sin(\omega\, t_N+\varphi) & t_n\rho_C\sin(\omega\, t_N+\varphi)\\ 0 & 0 & 1 & 0 & 0\\ 0 & 0 & 0 & 1 & 0\\ 0 & 0 & 0 & 0 & 1\end{bmatrix}$

is the Jacobian of the transformation $Z_N\mapsto Z$.

The CRLB of $Z_N$ (respectively of $Z$), denoted $B\left(Z_N|\theta_m\right)$ (respectively $B\left(Z|\theta_m\right)$), is the inverse of the FIM $F\left(Z_N|\theta_m\right)$ (respectively $F\left(Z|\theta_m\right)$). Note that because $\det\left(J_{Z,Z_N}\right)=1$, we have $\det\left[B\left(Z_N|\theta_m\right)\right]=\det\left[B\left(Z|\theta_m\right)\right]$ or in other words, the generalized variances are the same. As a consequence, the volumes of the confidence ellipsoids computed with the CRLB of $Z$ and of $Z_N$ are the same.

The orientation of the ellipsoid changes only in the 2D domain corresponding to the position (the first two components of $Z$ or $Z_N$).

### III.3 Performance of the MLE of the final range

The final range of the source is the parameter of greatest interest in practice. Moreover, it is a good indicator of the global behavior of the MLE in TMA problems. The accuracy of its estimate will be analyzed versus

- the final bearing,
- the final range (simply denoted $R_N$ in this section),
- and the duration of the observation.

Two characteristics of the performance will be used: the relative standard deviation (RSD) of the final range $\frac{\sigma_{R_N}}{R_N}$ computed from the CRLB and its relative empirical root-mean square error $\frac{RMSE_{R_N}}{R_N}$ evaluated from Monte Carlo simulations. The empirical root-mean square error is $RMSE_{R_N} \triangleq \sqrt{\frac{1}{L}\sum_{l=1}^{L}\left(\hat{R}_{N,l} - R_N\right)^2}$, $L$ being the number of accepted estimates and $\hat{R}_{N,l}$ being the estimated final range computed from the $l^{-th}$ accepted estimate $\hat{Z}_N$. The quantities $\frac{\sigma_{R_N}}{R_N}$ and the relative empirical root-mean square error (RERMSE) $\frac{RMSE_{R_N}}{R_N}$ are given in %.

In all the scenarios used in our simulations, the observer starts its trajectory at the origin; its speed and its heading are respectively 6 m/s and 90°. The trajectory of the source takes place in the upper half of plane ( $y \geq 0$ ). In this configuration, the source travels along the arc of a circle either clockwise ( $\omega > 0$ ), or anticlockwise ( $\omega < 0$ ). In all the figures, symbols + and o will represent the values of $\frac{RMSE_{R_N}}{R_N}$ for the clockwise case and the anti-clockwise case, respectively. The evolution of $\frac{\sigma_{R_N}}{R_N}$ vs. the parameter of interest will be drawn in continuous and dashed lines for clockwise and anticlockwise cases, respectively.

The standard deviation of the measurement is 0.5°; The standard deviation of the measurement is 0.5°; we chose $t_k = (k-1)\Delta t$ , with $\Delta t$ to be equal to 1 s.

The number of Monte Carlo runs is 500.

Remark:

Any other scenario can be deduced from these by an appropriate rotation or axial symmetry.

The performance of the estimated range is not changed by these isometries.

### *III.3.a Effects of the final bearing*

We have chosen a set of scenarios defined as follows:

- The source speed is $v_S = 5$ m/s.
- The trajectories of the source are identical up to a rotation around the final position of the observer (the angle of rotation is chosen to be equal to $\theta(t_N)$).
- The range of the center of the circle from the final position of the observer is 10 km, the radius $\rho_C$ being equal to 1 km.
- The initial angle $\varphi$ is chosen to be identical to the final bearing: $\varphi = \theta(t_N)$.
- The source makes a total turn, corresponding to a duration of 21 minutes (more precisely 1256 seconds, hence $N = 1256$ measurements).

Fig. 5 illustrates five particular scenarios where the source motion is clockwise. Symbol o shows the initial positions of each mobile.

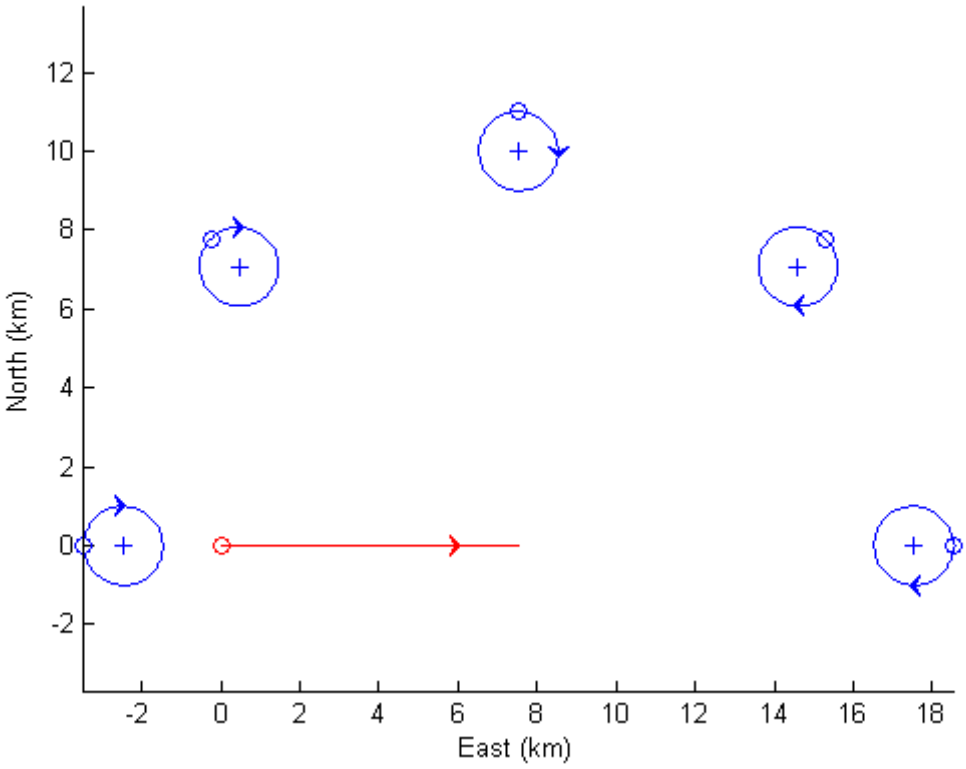


Fig. 5. Five scenarios for $v_S = 5$ m/s (clockwise cases).

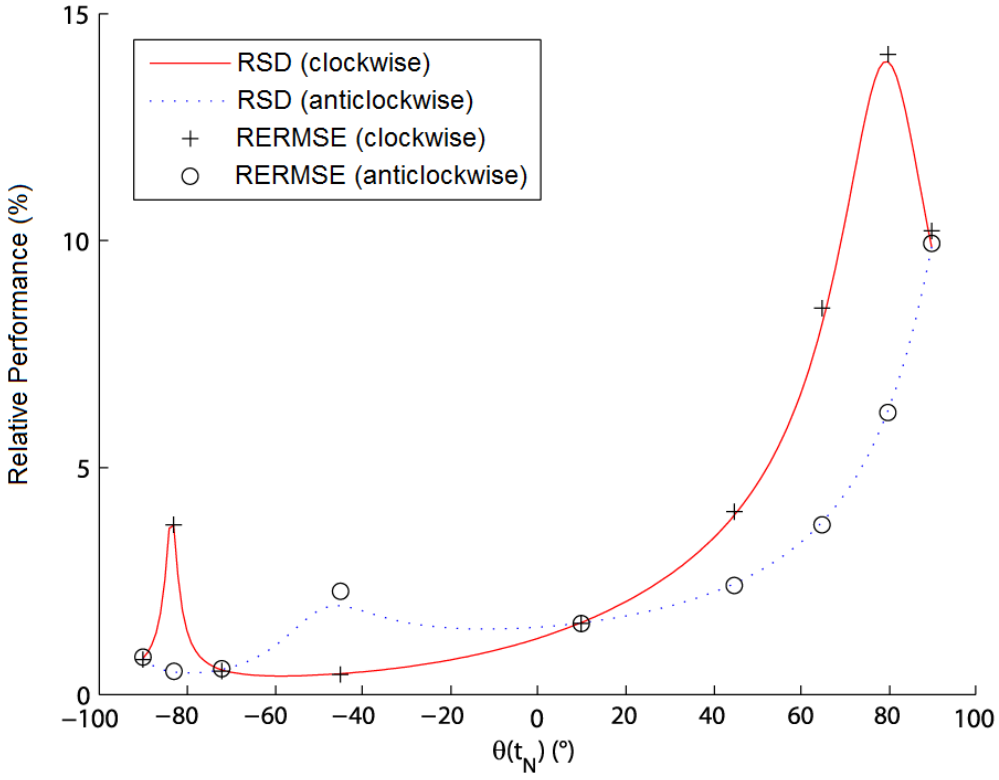


Fig. 6. $\frac{\sigma_{R_N}}{R_N}$ and $\frac{RMSE_{R_N}}{R_N}$ vs. the final bearing.

Fig. 6 depicts $\frac{\sigma_{R_N}}{R_N}$ and $\frac{RMSE_{R_N}}{R_N}$ vs. the final bearing for a set of nine scenarios.

The values of $\frac{RMSE_{R_N}}{R_N}$ are very close to the corresponding values of $\frac{\sigma_{R_N}}{R_N}$. The relative error being less than 15%, it is worth developing the BO-CTTMA for the chosen set of scenarios. The impact of the rotation direction on the CRLB hence on the performance of the MLE must be noted. This is due to the combination of two factors: the evolution of the bearings and of the range during the scenario.

### *III.3.b Effect of the final range*

In this part, we focus on the effect of the final range only. The set of scenarios is now defined as follows:

- the duration is still 1256 s,
- the final range between the final positions of the observer and of the source is taken in $\{5, 9, 13, 17, 21\}$ (km),
- the initial angle is taken in $\{-90, -45, 0, 45, 90\}$ (degree),
- $v_S = 5$ m/s and $\rho_C = 1$ km.

This set of scenarios is depicted in Fig. 7.

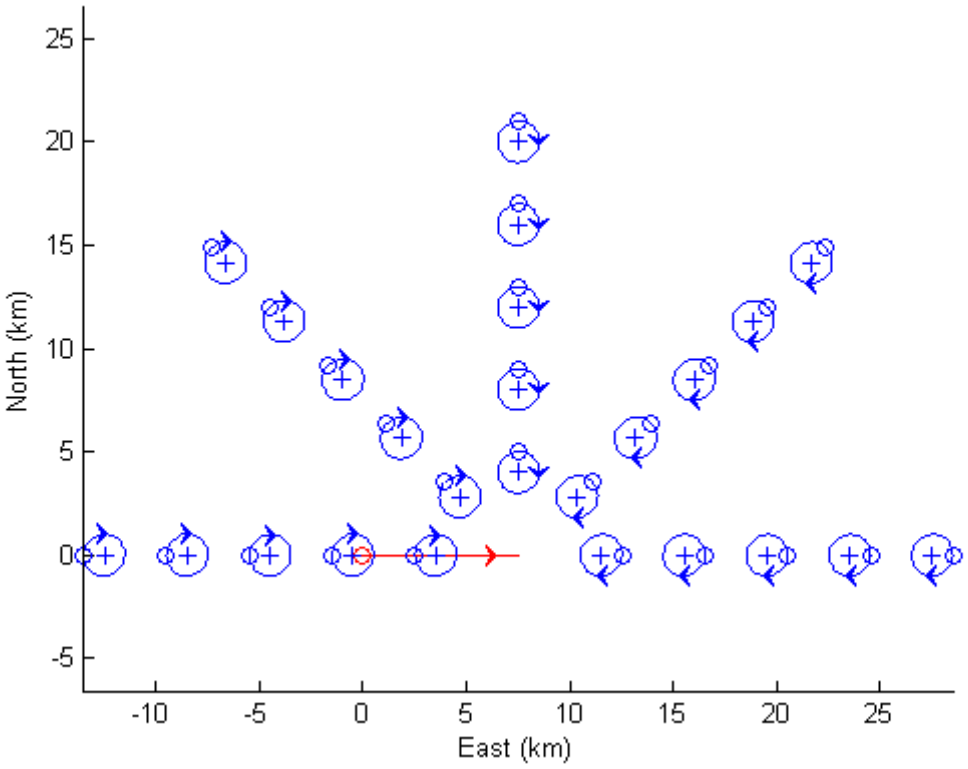


Fig. 7. Scenarios when $R_N$ is in $\{5, 9, 13, 17, 21\}$ (km) in the clockwise case.

The results are illustrated in Fig. 8: The values of $\frac{RMSE_{R_N}}{R_N}$ and $\frac{\sigma_{R_N}}{R_N}$ are very close and less than 10%, except the case where the final bearing is equal to 90° and when the final range is greater than 12 km. Again, the performance of the estimated range encourages us to study more deeply the BO-CTTMA. When the final bearing is equal to -90° or 90°, the values of $\frac{\sigma_{R_N}}{R_N}$ are the same for both turn rates (see Fig. 8.c).

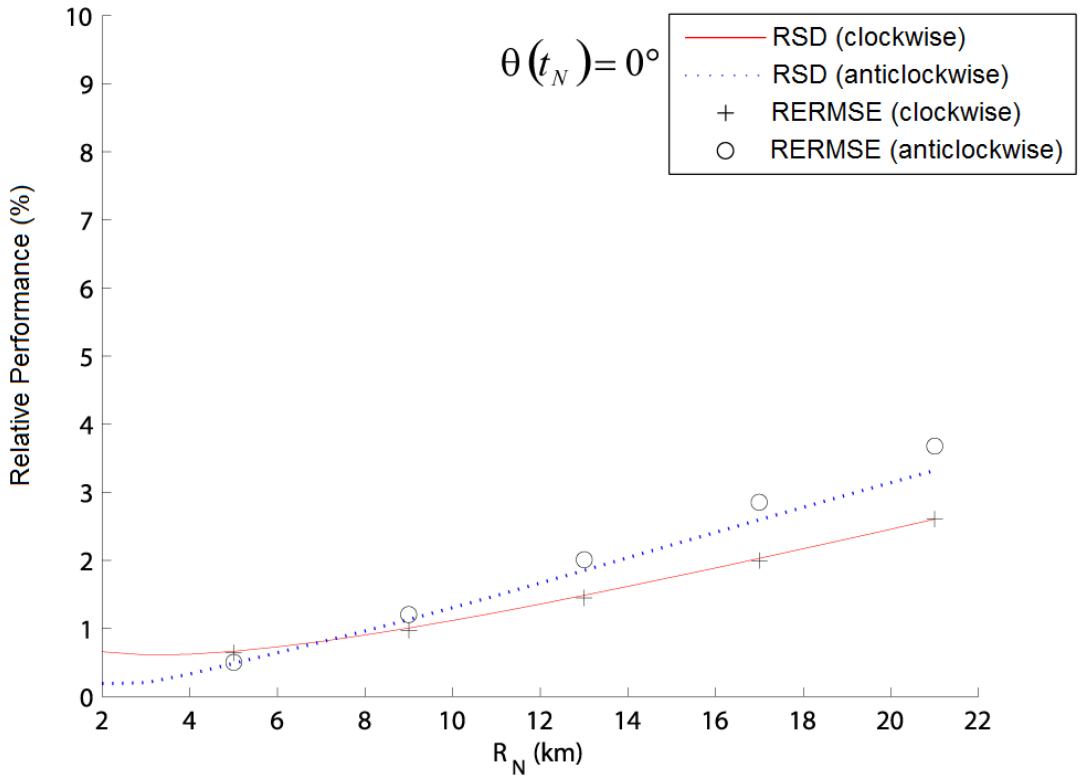


Fig. 8 (a). $\frac{\sigma_{R_N}}{R_N}$ and $\frac{RMSE_{R_N}}{R_N}$ vs. the final range when the bearing is 0°.

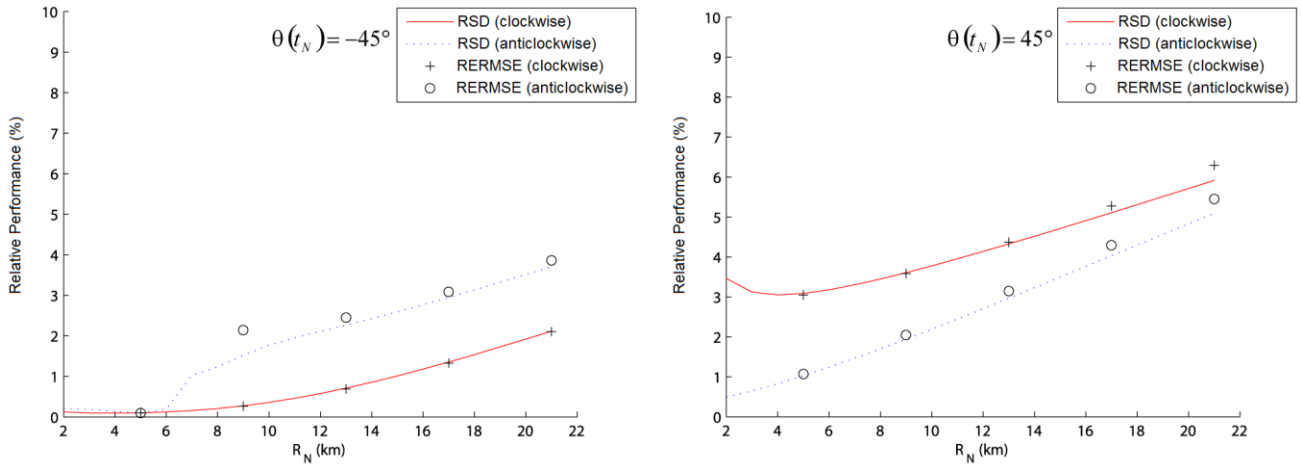


Fig. 8 (b). $\frac{\sigma_{R_N}}{R_N}$ and $\frac{RMSE_{R_N}}{R_N}$ vs. the final range when the initial bearing is -45° on the left, +45° on the right.

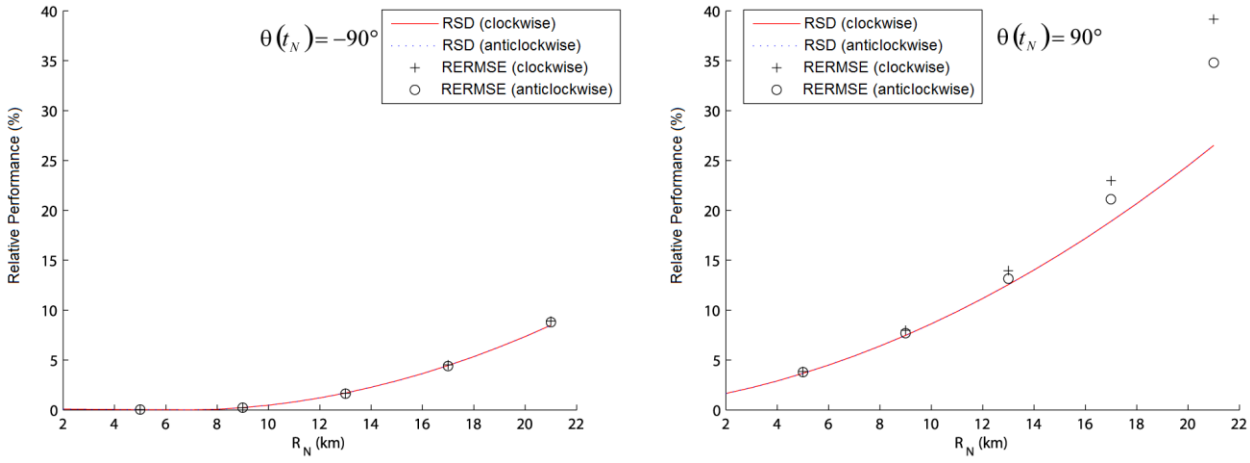


Fig. 8 (c). $\frac{\sigma_{R_N}}{R_N}$ and $\frac{RMSE_{R_N}}{R_N}$ vs. the final range when the initial bearing is -90° on the left, +90° on the right.

### *III.3.c Effect of the duration of the scenario only.*

To evaluate the effect of the duration, we use the scenarios presented in section III.3.a. Here only the duration changes: the minimum duration $t_N$ considered is 627 s (corresponding to a half turn), and the maximum is 1130 s (corresponding to 90 % of a total turn). Fig. 9 shows five scenarios for $t_N = 1130$ s and the direction is clockwise.

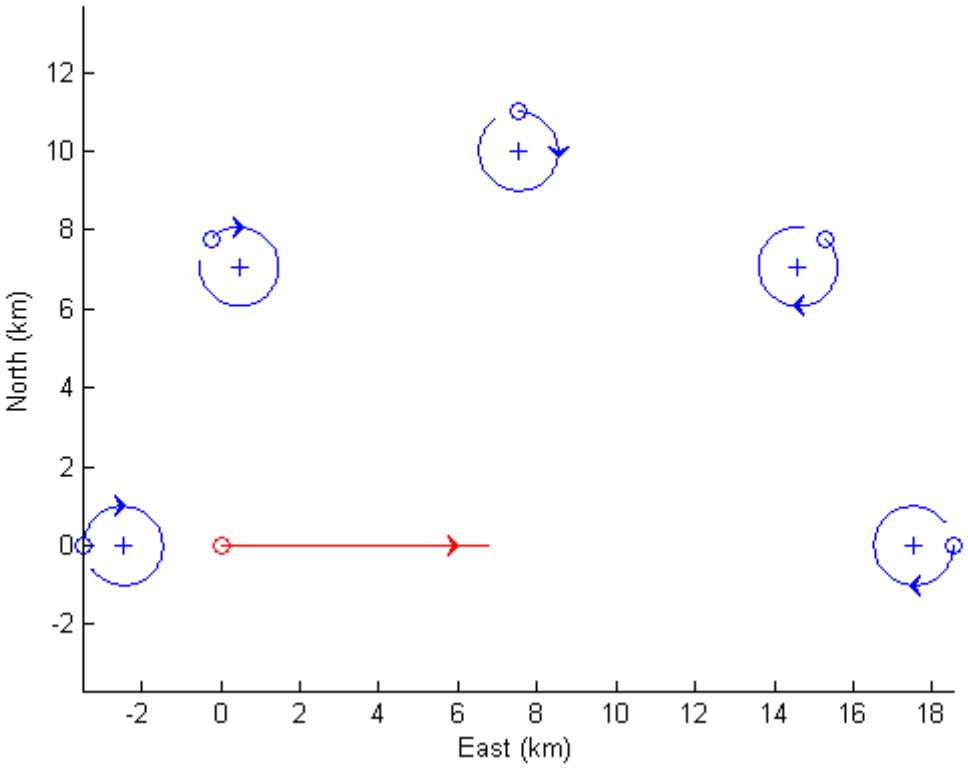


Fig. 9. Scenarios used to evaluate the performance of the MLE vs. the duration.

The results are shown in the five Fig. 10.

Except for the case where the initial angle is equal to 90°, the theoretical values $\frac{\sigma_{R_N}}{R_N}$ and empirical ones $\frac{RMSE_{R_N}}{R_N}$ are again very close. We note the great influence of the rotation direction: the performance in the clockwise case is three to five times better than in the anticlockwise case.

The "extreme" scenarios or end fire ($\varphi = -90°$ and $\varphi = 90°$) merit further comment: for the first one, the performance is excellent (less than 3%) whereas

in the second case the theoretical performance is the worse and the values of $\frac{RMSE_{R_N}}{R_N}$ are still much greater (up to 100%).

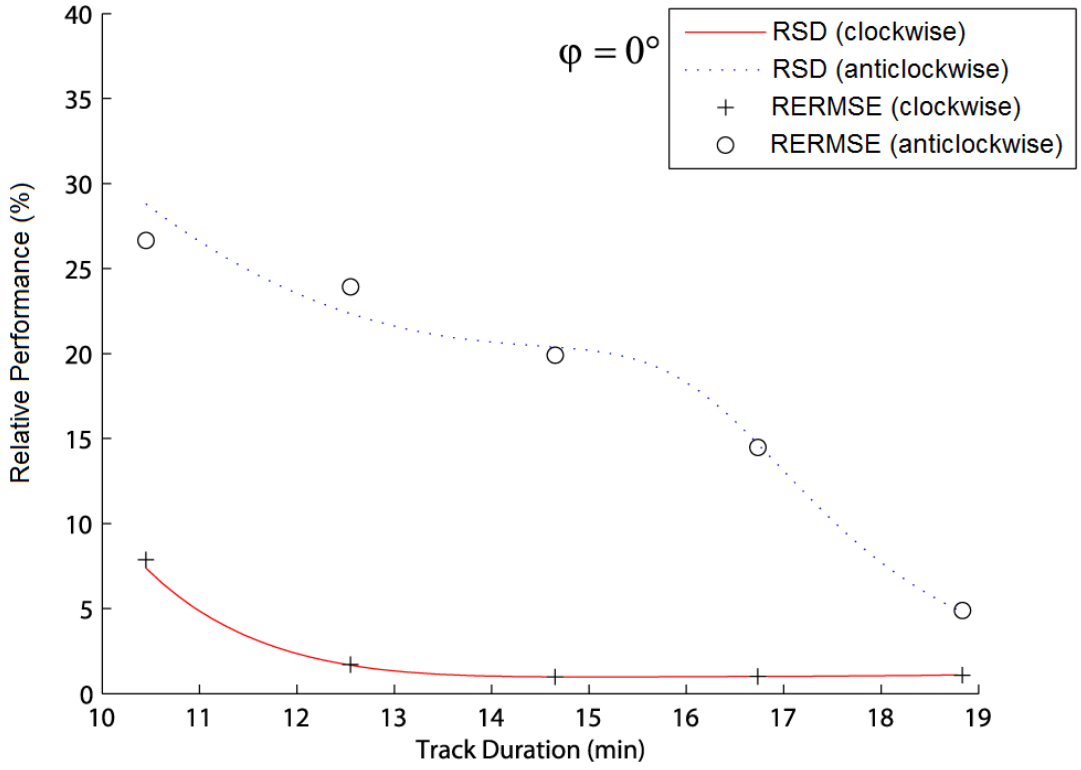


Fig. 10 (a). $\frac{\sigma_{R_N}}{R_N}$ and $\frac{RMSE_{R_N}}{R_N}$ vs. the track duration when the initial angle is 0°.

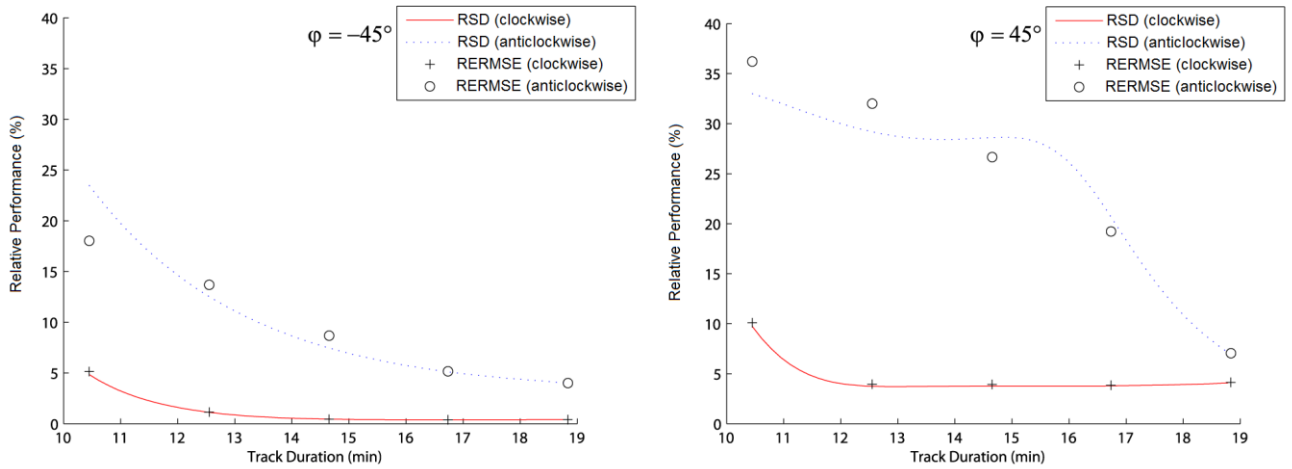


Fig. 10 (b). $\frac{\sigma_{R_N}}{R_N}$ and $\frac{RMSE_{R_N}}{R_N}$ vs. the track duration when the initial angle is -45°

on the left , +45° on the right.

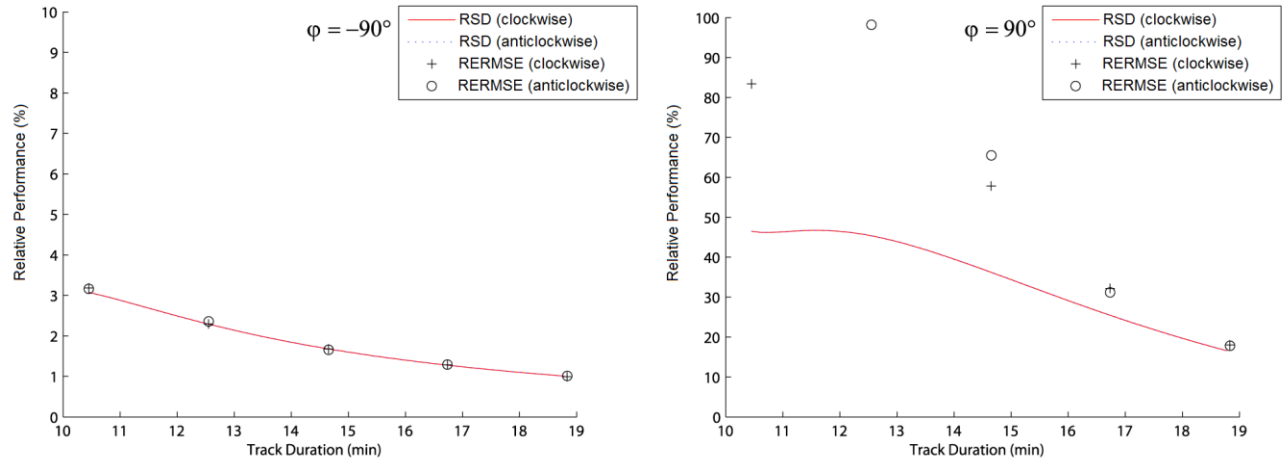


Fig. 10 (c). $\frac{\sigma_{R_N}}{R_N}$ and $\frac{RMSE_{R_N}}{R_N}$ vs. the track duration when the initial angle is -90°

on the left , +90° on the right

### III.4 Evaluation of the global performance of the MLE on a special scenario

We now focus on the scenarios depicted in Fig. 11 and Fig. 12 to detail the behavior of the estimator on each component of $Z_N$. The duration of the chosen scenarios is equal to 10 min. 27 s. (half of the complete circle is visited). The speed of the source and the radius of the circle keep their previous values, $v_S = 5$ m/s and $\rho_C = 1$ km.

These scenarios will be exploited in the coming section concerning the bearings and multi-frequencies TMA (see section IV.3.b).

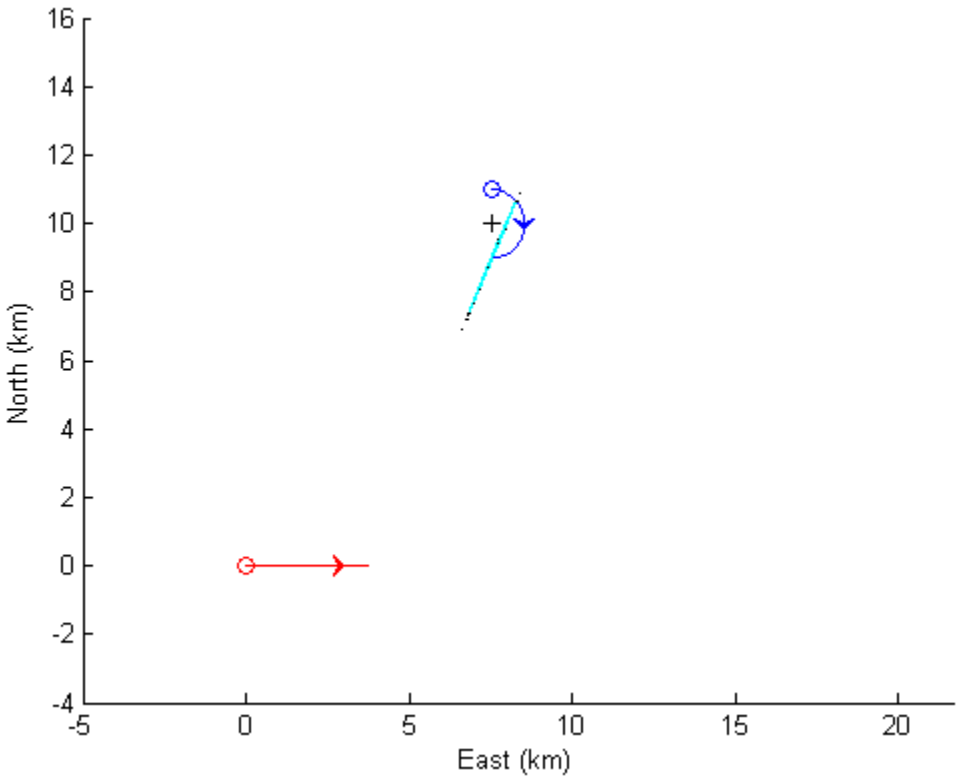


Fig. 11. Scenario together with the 95% confidence ellipsoid and estimated position (clockwise case).

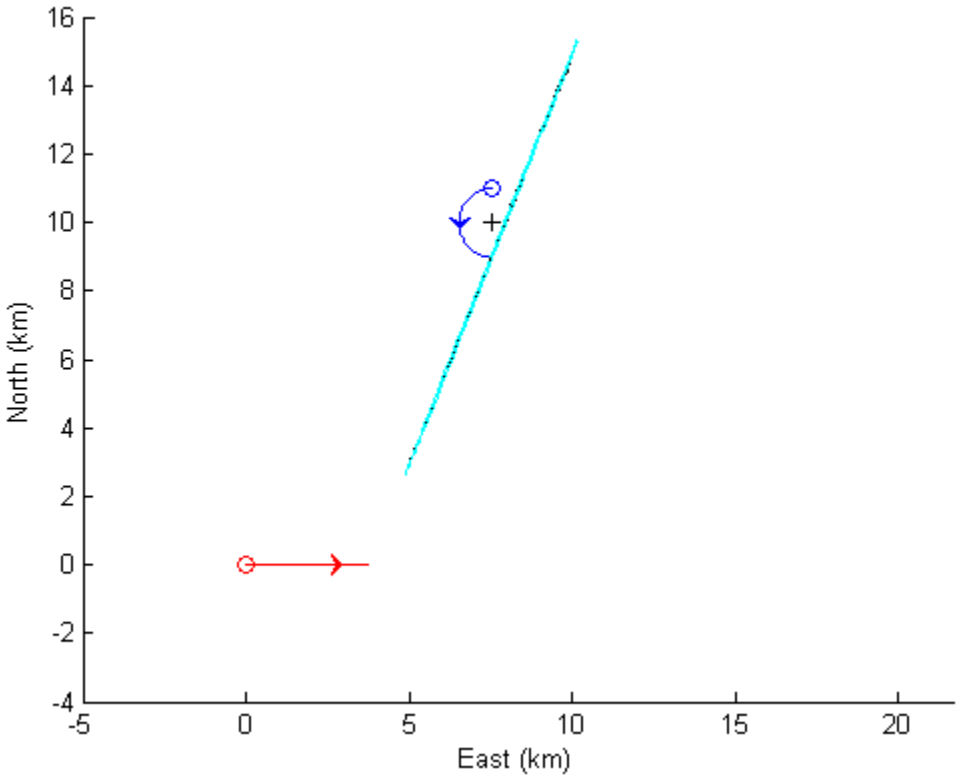


Fig. 12. Scenario together with the 95% confidence ellipsoid and estimated position (anticlockwise case).

The results of a 500 run simulation are presented in Fig. 11 and Fig. 12 (the confidence level of the ellipsoids is 95%). In the clockwise case, one estimate has been rejected by the test and seven have been rejected in the anticlockwise case.

The global statistics (concerning the accepted estimates only) are given in Table 1 and in Table 2. The column entitled $\sigma_{CRLB}$ contains the root square of the elements of the diagonal of the CRLB.

Table 1: Performance at final time (clockwise)

| | Units | True values | Bias | $\sigma_{CRLB}$ | $\hat{\sigma}$ |
|---|---|---|---|---|---|
| $x_S(t_N)$ | km | 7.54 | 0.02 | 0.29 | 0.29 |
| $y_S(t_N)$ | km | 9.00 | 0.03 | 0.65 | 0.66 |
| $\rho_C$ | km | 1.00 | 0.04 | 0.09 | 0.10 |
| $\varphi$ | ° | 0.00 | 0.47 | 7.28 | 7.35 |
| $\omega$ | °/s | 0.287 | 0.002 | 0.025 | 0.026 |
| $R_N$ | km | 9.76 | 0.03 | 0.71 | 0.72 |

Table 2 : Performance at final time (anticlockwise)

| | Units | True values | Bias | $\sigma_{CRLB}$ | $\hat{\sigma}$ |
|---|---|---|---|---|---|
| $x_S(t_N)$ | km | 7.52 | 0.22 | 1.08 | 1.22 |
| $y_S(t_N)$ | km | 9.00 | 0.52 | 2.59 | 2.92 |
| $\rho_C$ | km | 1.00 | 0.04 | 0.25 | 0.23 |
| $\varphi$ | ° | 0.00 | 32.7 | 28.5 | 60.7 |
| $\omega$ | °/s | -0.287 | 0.123 | 0.06 | 0.236 |
| $R_N$ | km | 9.76 | 0.57 | 2.81 | 3.22 |

- clockwise case

Less than 11 iterations are needed to ensure convergence. The bias of each component of the estimated state vector is negligible and the proximity between $\sigma_{CRLB}$ and $\hat{\sigma}$ allows us to conclude that the MLE is efficient.

- anticlockwise case

  Convergence is obtained with less than 15 iterations. Unlike the clockwise case, the bias of the last two components of the state vector (the initial angle $\varphi$ and the turn rate $\omega$) are not negligible; moreover the empirical standard deviation is not close to $\sigma_{CRLB}$. So, we cannot conclude that the MLE is efficient. However, the first three components are efficiently estimated.

# IV Exploitation of additional frequency measurements (FB-CTTMA and MFB-CTTMA)

In a passive sonar system, additional measurements are often available; most commonly frequencies, which contain information about the trajectory of the source thanks to the Doppler effect.

In this section we propose to evaluate the potential gain of one or more frequency tracks in the BO-CTTMA. This new method will be denoted FB-CTTMA (for bearings-frequencies TMA in constant turn) or MFB-CTTMA (for bearings-

multifrequencies TMA in constant turn). Such as in the BO-CTTMA, we start with a recall of hypothesis and notations. Then we will study observability of the MFB-CTTMA, compare its performance to that of the BO-CTTMA and introduce the MLE corresponding to this last case.

## IV.1 FB-CTTMA

### *IV.1.a Notations*

The kinematics of the platform are identical to those given in §II.1: the observer moves with a constant velocity while the source follows a circular trajectory at constant speed. This time, the source emits a single pure tone with constant and unknown frequency $f_0$ . The state vector is now defined as follows:

$$Y = \begin{bmatrix} f_0 & x_C & y_C & \rho_C & \varphi & \omega \end{bmatrix}^T = \begin{bmatrix} f_0, Z^T \end{bmatrix}^T \qquad (2)$$

where $f_0$ is the unknown emitted frequency.

The noise-free received frequency is at time $t$

$$f(t) = f_0 \left[ 1 - \dot{R}(t) / C \right] \qquad (3)$$

where $\dot{R}(t)$ is the radial component of the relative speed at time $t$ and $C$ is the speed of sound in the medium (about 1500 m/s in water). The radial speed is expressed in terms of $Z$:

$$\dot{R}(t) = (\dot{x}_S(t) - \dot{x}_O)\sin\theta(Z,t) + (\dot{y}_S(t) - \dot{y}_O)\cos\theta(Z,t)$$

where $[\dot{x}_O \quad \dot{y}_O]^T$ is the observer's velocity vector and $[\dot{x}_S(t) \quad \dot{y}_S(t)]^T$ is the source's velocity vector at time $t$, more precisely:

$$\dot{x}_S(t) = \rho_C\omega\cos(\omega t + \varphi) \text{ and } \dot{y}_S(t) = -\rho_C\omega\sin(\omega t + \varphi).$$

In order to emphasize the relationship between $Y$ and the noise-free frequency, we will write $f(Y,t)$ instead of $f(t)$.

Under those assumptions, the FB-CTTMA consists of estimating $Y$ from a collection of pairs of measurements

$$\begin{cases} \theta_m(t_k) = \theta(Z,t_k) + \varepsilon_\theta(t_k) \\ f_m(t_k) = f(Y,t_k) + \varepsilon_f(t_k) \end{cases} \text{ for } k = 1,\ldots,N$$

where $\varepsilon_\theta(t_k)$ and $\varepsilon_f(t_k)$ are the additive noises that corrupt the bearing and frequency measurements, respectively. In the sequel, these noises are assumed to be independent, 0-mean Gaussian and their standard deviations are $\sigma_\theta(t_k)$ and $\sigma_f(t_k)$, respectively, assumed to be known.

### *IV.1.b Observability in FB-CTTMA*

In §II.2, the observability conditions in the BO-CTTMA case have been given: the only case of non-observability is met when the observer is motionless. So, the first question we have to answer is: does taking into account frequency measurements make the source in CT motion observable when the observer is stationary?

The answer is given by the following result.

RESULT 5

*Assume that the observer is motionless.*

*Any source in CT motion is observable from bearings and frequencies measurements if and only if the observer is not located at the center of the circle traveled by the source.*

The proof of the result is given in the appendix §VII.2.

## IV.2 MFB-CTTMA

### *IV.2.a Notations*

In this section, the source is supposed to emit $P$ constant and unknown frequencies $f_0, f_1, \cdots, f_{P-1}$. The state vector is now

$$Y = \left[ f_0, f_1, \cdots, f_p, \cdots, f_{P-1}, Z^T \right]^T .$$

The $P$ measured frequencies are given by

$$f_{p,m}(t_k) = f_p(Y, t_k) + \varepsilon_{f_p}(t_k), \quad \text{for } p = 0, 1, \cdots, P-1,$$

with, as previously (3)

$f_p(Y, t_k) = f_p\left[1 - \dot{R}(t_k)/C\right]$ .

The variance of $\varepsilon_{f_p}(t_k)$ is denoted $\sigma^2_{f_p}(t_k)$.

The set of frequency measurements corresponding to the pure frequency $f_p$ is

$f_{p,m} = \left\{f_{p,m}(t_1),\ f_{p,m}(t_2),\ f_{p,m}(t_3), \cdots, f_{p,m}(t_N)\right\}$, for $p = 0,1,\cdots,P-1$.

### *IV.2.b CRLB in MFB-CTTMA*

Taking into account extra measurements (the frequencies) implies augmenting the dimension of the state vector, hence the number of unknowns. In this sense, the unknown emitted frequencies $f_0, f_1,\cdots, f_{P-1}$ to estimate play the role of nuisance parameters: in short we have more information but more unknowns. So, the fundamental question of the MFB-CTTMA is the following:

*Does the MFB-CTTMA improve the accuracy of the estimate of $Z$ (parameter concerning the trajectory only)? In terms of the Cramér-Rao lower bound, the question is*

$B\left(Z|\theta_m, f_{0,m},\cdots, f_{P-1,m}\right) \preceq B\left(Z|\theta_m, f_{0,m}\right) \preceq B\left(Z|\theta_m\right)$ ? (4)

Remarks:

- If $M_1$ and $M_2$ are two positive definite symmetric matrices, then $M_1 \preceq M_2$ means that $M_2 - M_1$ is a positive semidefinite matrix.
- We implicitly assume that there is one single bearing measurement, the same one for all the frequencies at each sampling time. In reality, a

measured frequency is always coupled to a measured bearing. Hence, we should have as many bearings as frequencies. Because all these bearings are relative to the same line of sight, they are averaged and the result is a more accurate single measured bearing. In order to make a fair comparison, the standard deviation of the bearing has been kept at the same value. So, the impact of the extra frequency lines will be objectively judged.

- The bearing rate is supposed to be not equal to zero.
- The numbering of the frequencies is arbitrary.

Under all the specified assumptions given in this section, we obtain the following result.

RESULT 6

*The performance of the estimation of the sub-state-vector* $Z$ *(concerning the trajectory only) is improved with increase of the number of (unknown) frequencies included in the state vector* $Y$*. This property can be summarized by the following inequality, in terms of CRLB:*

$$B\left(Z\middle|\theta_m, f_{0,m},\cdots, f_{P-1,m}\right) \preceq B\left(Z\middle|\theta_m, f_{0,m},\cdots, f_{P-2,m}\right) \preceq \cdots \preceq B\left(Z\middle|\theta_m, f_{0,m}\right) \preceq B\left(Z\middle|\theta_m\right).$$

Remark:

This result was obtained previously when the source was in CV motion (see [22])

## IV.3 MLE in MFB-CTTMA

### *IV.3.a Numerical aspects*

We choose the MLE which consists of minimizing the following quadratic criterion

$$C(Y)=\sum_{k=1}^{N}\left[\frac{\theta_m(t_k)-\theta(Z,t_k)}{\sigma_\theta(t_k)}\right]^2+\sum_{p=0}^{P-1}\sum_{k=1}^{N}\left[\frac{f_{p,m}(t_k)-f_p(Y,t_k)}{\sigma_{f_p}(t_k)}\right]^2$$

As previously, we employ the Gauss-Newton routine. The initial point $\bar{Y}=\left[\bar{f}_0,\bar{f}_1,\cdots,\bar{f}_p,\cdots,\bar{f}_{P-1},\bar{Z}^T\right]^T$ is selected as follows:

- $\bar{Z}$ is a node of a coarse grid,
- Each $\bar{f}_p$ is equal to the mean value of each track.

The returned $\hat{Y}$ is accepted if $C(\hat{Y})$ is less than $N-5+P(N-6))+3\sqrt{(2N-10)}+3P\sqrt{(2N-12)}$ (99.5% of the population). Then, we compute the corresponding $\hat{Y}_N=\left[\hat{f}_0,\hat{f}_1,\cdots,\hat{f}_p,\cdots,\hat{f}_{P-1},\hat{Z}_N^T\right]^T$.

### *IV.3.b Monte Carlo simulations*

The scenarios used in § III.4 are used here. Now, the target emits $P$ constant frequencies $(P=1,2,4)$. The emitted frequencies are:

- $P=1$: $f_0=3$ kHz.
- $P=2$: $f_0=3$ kHz and $f_1=3.5$ kHz.
- $P=4$: $f_0=3$ kHz, $f_1=3.5$ kHz, $f_2=4$ kHz and $f_3=4.5$ kHz.

- The standard deviation of each frequency track is equal to $\sigma_{f_p} = f_p / 1000$ Hz for each $p$.
- The celerity in the medium is $C = 1500$ m/s.

### IV.3.b.1 Clockwise case

The two following tables contain the performance of the MLE for each value of $P$: In Table 3 the mean values of the estimates are listed while in Table 4 the empirical standard deviation is given. The column “Bearings only” corresponds to the previous results obtained in § III.4 for the bearings-only case.

Table 3: Bias of the MLE (clockwise)

| | | | Bearings only | | One freq. | | Two freq. | | Four freq. | |
|---|---|---|---|---|---|---|---|---|---|---|
| $Z_N$ | Units | $Z_{N\,True}$ | $\hat{Z}_{N\,Average}$ | Bias | $\hat{Z}_{N\,Average}$ | Bias | $\hat{Z}_{N\,Average}$ | Bias | $\hat{Z}_{N\,Average}$ | Bias |
| $x_S(t_N)$ | km | 7.54 | 7.52 | 0.02 | 7.53 | 0.01 | 7.53 | 0.01 | 7.53 | 0.01 |
| $y_S(t_N)$ | km | 9 | 8.97 | 0.03 | 9.00 | 0.00 | 9.00 | 0.00 | 9.00 | 0.00 |
| $\rho_C$ | km | 1 | 1.04 | 0.04 | 1.00 | 0.00 | 1.00 | 0.00 | 1.00 | 0.00 |
| $\varphi$ | ° | 0 | 0.47 | 0.47 | 0.06 | 0.06 | -0.04 | 0.04 | -0.06 | 0.06 |
| $\omega$ | °/s | 0.288 | 0.286 | 0.002 | 0.287 | 0.001 | 0.287 | 0.001 | 0.287 | 0.001 |

Table 4: Theoretical and empirical standard deviations of the MLE (clockwise)

| | | | Bearings only | | One freq. | | Two freq. | | Four freq. | |
|---|---|---|---|---|---|---|---|---|---|---|
| $Z_N$ | Units | $Z_{N\,True}$ | $\sigma_{CRLB}$ | $\hat{\sigma}$ | $\sigma_{CRLB}$ | $\hat{\sigma}$ | $\sigma_{CRLB}$ | $\hat{\sigma}$ | $\sigma_{CRLB}$ | $\hat{\sigma}$ |
| $x_S(t_N)$ | km | 7.54 | 0.29 | 0.29 | 0.09 | 0.09 | 0.07 | 0.73 | 0.06 | 0.06 |
| $y_S(t_N)$ | km | 9 | 0.65 | 0.66 | 0.20 | 0.20 | 0.15 | 0.15 | 0.12 | 0.12 |
| $\rho_C$ | km | 1 | 0.09 | 0.1 | 0.04 | 0.04 | 0.03 | 0.03 | 0.03 | 0.03 |
| $\varphi$ | ° | 0 | 7.28 | 7.35 | 2.79 | 2.79 | 2.23 | 2.29 | 1.81 | 1.84 |
| $\omega$ | °/s | 0.288 | 0.026 | 0.026 | 0.077 | 0.077 | 0.006 | 0.006 | 0.005 | 0.005 |

We observe that the bias is negligible on each component of $Z_N$ and the empirical standard deviations are very close to the values deduced from the CRLB. The MLE is hence efficient. Moreover, the more frequencies taken into account, the more accurate the estimates will be.

### IV.3.b.2 Anticlockwise case

Table 5 : Bias of the MLE (anticlockwise)

| | Bearings only | One freq. | Two freq. | Four freq. |
|---|---|---|---|---|

| $Z_N$ | Units | $Z_{N\,True}$ | $\hat{Z}_{N\,Average}$ | Bias | $\hat{Z}_{N\,Average}$ | Bias | $\hat{Z}_{N\,Average}$ | Bias | $\hat{Z}_{N\,Average}$ | Bias |
|---|---|---|---|---|---|---|---|---|---|---|
| $x_S(t_N)$ | km | 7.52 | 7.74 | 0.22 | 7.53 | 0.01 | 7.53 | 0.01 | 7.53 | 0.01 |
| $y_S(t_N)$ | km | 9.00 | 9.52 | 0.52 | 8.99 | 0.01 | 8.99 | 0.01 | 9.00 | 0.00 |
| $\rho_C$ | km | 1.00 | 1.04 | 0.04 | 1.00 | 0.00 | 1.00 | 0.00 | 1.00 | 0.00 |
| $\varphi$ | ° | 0.00 | -32.7 | 32.7 | 0.05 | 0.05 | 0.09 | 0.09 | -0.04 | 0.04 |
| $\omega$ | °/s | -0.287 | -0.164 | 0.123 | -0.287 | 0.000 | -0.287 | 0.000 | -0.287 | 0.000 |

Table 6 : Theoretical and empirical standard deviations of the MLE

(anticlockwise)

| | | | Bearings only | | One freq. | | Two freq. | | Four freq. | |
|---|---|---|---|---|---|---|---|---|---|---|
| $Z_N$ | Units | $Z_{N\,True}$ | $\sigma_{CRLB}$ | $\hat{\sigma}$ | $\sigma_{CRLB}$ | $\hat{\sigma}$ | $\sigma_{CRLB}$ | $\hat{\sigma}$ | $\sigma_{CRLB}$ | $\hat{\sigma}$ |
| $x_S(t_N)$ | km | 7.52 | 1.08 | 1.22 | 0.11 | 0.11 | 0.08 | 0.08 | 0.06 | 0.06 |
| $y_S(t_N)$ | km | 9 | 2.59 | 2.92 | 0.26 | 0.26 | 0.19 | 0.19 | 0.15 | 0.15 |
| $\rho_C$ | km | 1 | 0.248 | 0.227 | 0.046 | 0.048 | 0.038 | 0.038 | 0.033 | 0.034 |
| $\varphi$ | ° | 0 | 28.5 | 60.7 | 3 | 3.1 | 2.2 | 2.3 | 1.6 | 1.6 |
| $\omega$ | °/s | -0.287 | 0.060 | 0.236 | 0.009 | 0.009 | 0.007 | 0.007 | 0.005 | 0.005 |

As we observe in section III.4, the MLE for the BO-CTTMA problem is not efficient, in the anticlockwise case. The efficiency of the MLE is obtained as soon as at least one frequency track is available.

In both cases, the simulations confirm the inequalities of RESULT 6.

# V To maneuver or not to maneuver?

We start this last section with a comparison of the performance of TMA when two platforms try to track each other from bearings only (each of them is the “source” of the other). One platform has a constant velocity vector while the other one travels on an arc of a circle. In this contest, the first one employs the technique of BO-CTTMA and the second carries out the classical BO-TMA.

Then, we extend this study when an additional frequency measurement is available for each platform.

## V.1 BO-TMA against BO-CTTMA

The chosen scenario is the one used in section III.4 for the anticlockwise turn. The duration ($t_N$) goes from 753 seconds (60% of a turn) to 1130 seconds (90% of a turn). During the whole scenario, the standard deviation does not change: $\sigma_\theta = 0.5°$ (for each platform).

Fig. 13 depicts the MLE of each method together with their respective 95% confidence ellipsoids for different durations as mentioned in Table 7. The performance is analyzed via the values of $\frac{\sigma_{R_N}}{R_N}$ and $\frac{RMSE_{R_N}}{R_N}$.

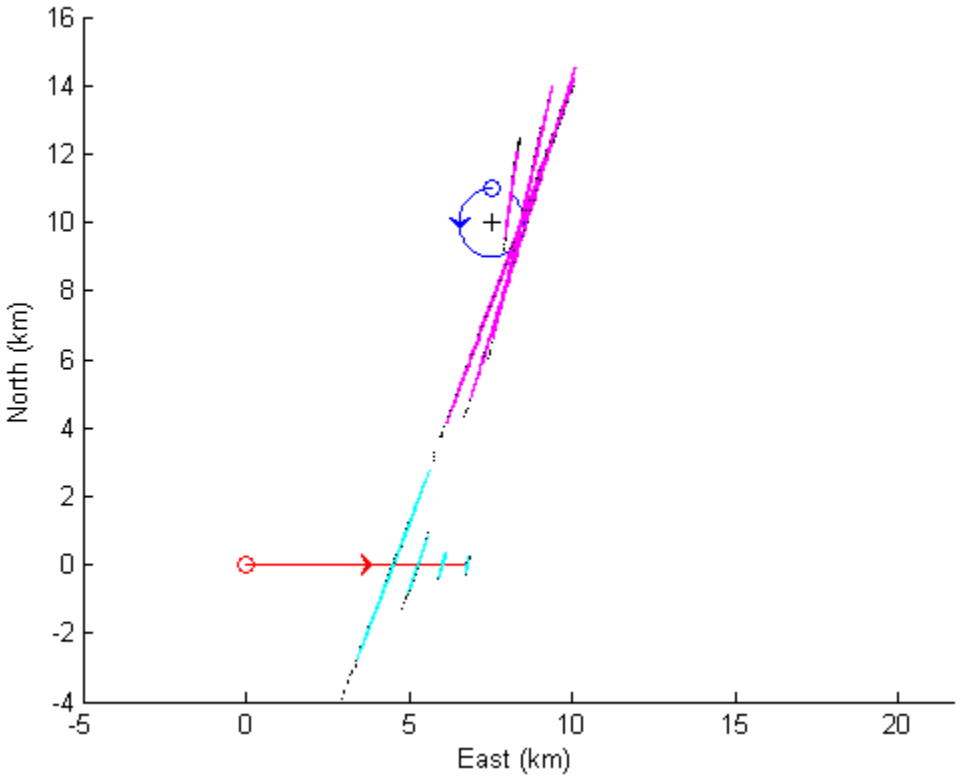


Fig. 13. Scenario used for the comparison between BO-TMA and BO-CTTMA.

From Table 7 and Fig. 13, the MLE of the BO-TMA performs better than the MLE in BO-CTTMA. Moreover, the duration of the scenario must be longer for the non-maneuvering platform to reach a good accuracy: in this scenario, a complete turn is necessary to obtain acceptable performance (about 5%). In conclusion, when bearings only are available, the tactical advantage is for the maneuvering platform.

Table 7 : Respective performance of BO-TMA and BO-CTTMA (in %)

| Duration (s) | 753 | | 879 | | 1004 | | 1130 | |
|---|---|---|---|---|---|---|---|---|
| | $\frac{\sigma_{R_N}}{R_N}$ | $\frac{RMSE_{R_N}}{R_N}$ | $\frac{\sigma_{R_N}}{R_N}$ | $\frac{RMSE_{R_N}}{R_N}$ | $\frac{\sigma_{R_N}}{R_N}$ | $\frac{RMSE_{R_N}}{R_N}$ | $\frac{\sigma_{R_N}}{R_N}$ | $\frac{RMSE_{R_N}}{R_N}$ |
| BO-TMA | 12.29% | 12.65% | 3.58% | 3.56% | 1.46% | 1.44% | 0.81% | 0.81% |
| BO-CTTMA | 22.35% | 28.33% | 20.38% | 22.54% | 14.70% | 16.66% | 4.79% | 6.26% |

## V.2 FB-TMA against FB-CTTMA

We are going to evaluate the interest of taking into account a frequency track in the same scenario. So the maneuvering platform will use the FB-TMA and the non-maneuvering platform the FB-CTTMA (for each method, the MLE is computed).

The only difference is that the shortest duration ($t_N$) is 627 seconds (50% of a turn).

The emitted frequency is $f_0 = 3$ kHz. During the whole scenario, the measurements keep the same standard deviation: $\sigma_{f_0} = 3$ Hz and $\sigma_\theta = 0.5°$ (for each platform).

Again, the respective performance is presented in a figure and a table: on Fig. 14, the estimates and their 95% confidence ellipsoids are drawn while in Table 8 the values of $\frac{\sigma_{R_N}}{R_N}$ and $\frac{RMSE_{R_N}}{R_N}$ are given.

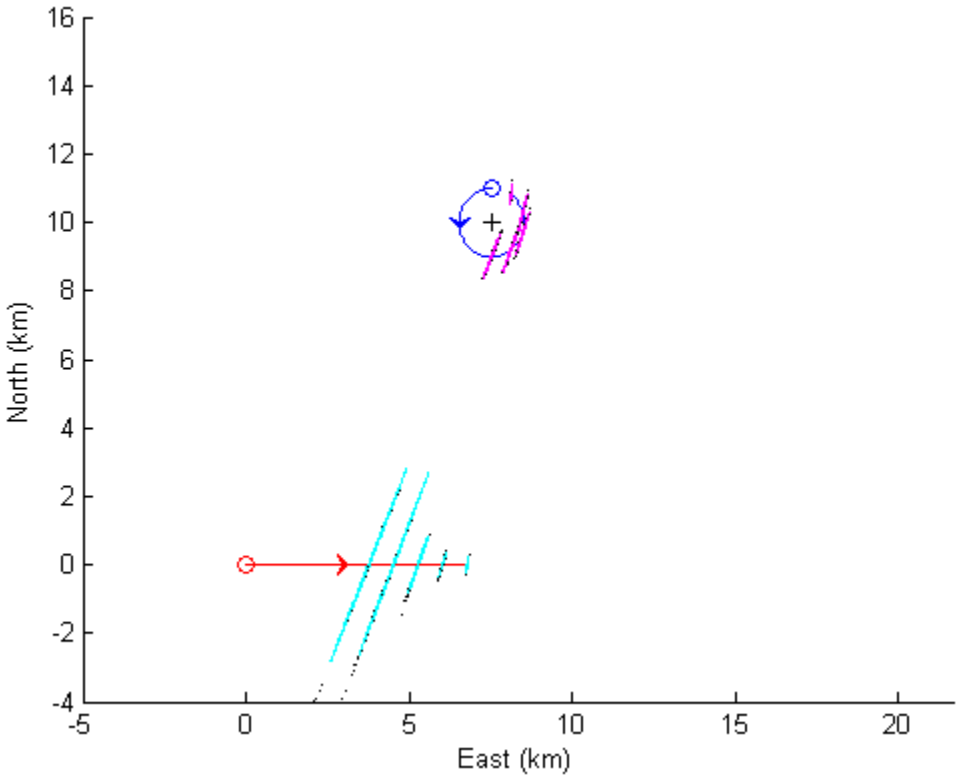


Fig. 14. Scenario used for the comparison between FB-TMA and FB-CTTMA.

The results show that the previous conclusion is no longer valid: if a frequency track is used together with bearings, the non-maneuvering platform obtains much better performance than the maneuvering platform. Moreover, in the both methods, the MLE is consistent whatever the scenario duration.

Table 8 : Respective performance of FB-TMA and FB-CTTMA (in %).

| Duration (s) | 627 | | 753 | | 879 | | 1004 | | 1130 | |
|---|---|---|---|---|---|---|---|---|---|---|
| | $\frac{\sigma_{R_N}}{R_N}$ | $\frac{RMSE_{R_N}}{R_N}$ | $\frac{\sigma_{R_N}}{R_N}$ | $\frac{RMSE_{R_N}}{R_N}$ | $\frac{\sigma_{R_N}}{R_N}$ | $\frac{RMSE_{R_N}}{R_N}$ | $\frac{\sigma_{R_N}}{R_N}$ | $\frac{RMSE_{R_N}}{R_N}$ | $\frac{\sigma_{R_N}}{R_N}$ | $\frac{RMSE_{R_N}}{R_N}$ |

| | | | | | | | | | | |
|---|---|---|---|---|---|---|---|---|---|---|
| FB-TMA | 12.75% | 12.71% | 11.90% | 11.65% | 3.58% | 3.75% | 1.46% | 1.41% | 0.81% | 0.81% |
| FB-CTTMA | 2.86% | 2.99% | 2.73% | 2.78% | 2.60% | 2.63% | 2.04% | 1.85% | 1.13% | 1.03% |

Remark: these conclusions must be verified using a range of scenarios to be confirmed definitely.

## VI Conclusion

In this paper, we have considered a source in constant turn motion and an observer with a constant velocity vector.

Firstly, its observability has been analyzed when the observer measures bearings only: the trajectory of the source is observable, except when the observer is motionless. If the observer is motionless and not located in the circle in which the source is moving, then the set of trajectories detected in the same lines of sight are all homothetic. In this case, if the observer acquires an additional frequency measurement, then the system becomes observable.

Any trajectory of a target composed of a succession of legs and at least an arc of a circle is observable from a non-maneuvering observer.

Concerning the estimation aspect, the MLE has sufficient performance to present a practical interest in anti-submarine warfare. This performance is close to the CRLB. These results have been obtained with a set of representative scenarios.

Taking frequency measurements into account improves the accuracy of the estimator (the more frequencies, the better the accuracy).

Finally, a comparison between the performance of TMA of a maneuvering observer and a non-maneuvering one has been made: when only bearings are used, the maneuvering observer has advantage over the non-maneuvering one. This is inverted when both acquire bearing and frequency measurements.

In the future, the robustness of the MLE merits to be studied when the assumption of constant speed is violated which is possible in reality as shown in [26] for a surface ship. Note that we have presented some preliminary results in [12]. The robustness against biased bearing measurements must also be treated. Another axis of research concerns the model tests whose aim will be to choose the more appropriate source kinematic (between CT and CV). The extension to the 3D case is conceivable for aerospace applications in angle only or with additional frequency [24][25].

***Acknowledgement:*** *The authors are grateful to Frederic Dambreville for his expertize regarding the proof of RESULT 2, and to the anonymous reviewers for their constructive suggestions.*

# VII Appendix

We need the following result for the so called “analytic continuation” [27] .

Proposition

*Let* $g$ *and* $h$ *be two analytic functions on* $\mathbb{R}$ *and* $U$ *an open interval in* $\mathbb{R}$*.*

*If* $g(x)=h(x)$ *for any* $x\in U$*, then* $g(x)=h(x)$ *for any* $x\in\mathbb{R}$*.*

## VII.1 Proofs of Results 1, 2 and 3

With no loss of generality and for the sake of simplicity, we will assume that the observer is moving along the x-axis, *i.e.* $\begin{bmatrix} x_O(t) \\ y_O(t) \end{bmatrix} = \begin{bmatrix} t\,\dot{x}_O \\ 0 \end{bmatrix}$ during $[0, T]$ or is stationary ($\dot{x}_O = 0$).

We need to ascertain the existence of another source, denoted $S'$, detected in the same bearing $\theta(t)$ as $S$ by the observer during $[0, T]$. Its position at time $t$ being $\begin{pmatrix} x_{S'}(t) \\ y_{S'}(t) \end{pmatrix}$, we get

$$\theta(t) = \arg\begin{pmatrix} x_S(t) - x_O(t) \\ y_S(t) \end{pmatrix} = \arg\begin{pmatrix} x_{S'}(t) - x_O(t) \\ y_{S'}(t) \end{pmatrix}, \quad \forall t \in [0, T] \qquad (5)$$

$\Leftrightarrow$ A positive scalar $\lambda(t)>0$ exists such that

$$\frac{x_S(t)-t\,\dot{x}_O}{y_S(t)}=\frac{\lambda(t)\left[x_{S'}(t)-t\,\dot{x}_O\right]}{\lambda(t)y_{S'}(t)},\qquad \forall t\in\left[0,\,T\right]$$

which implies that $\left[x_S(t)-t\,\dot{x}_O\right]y_{S'}(t)=\left[x_{S'}(t)-t\,\dot{x}_O\right]y_S(t),\qquad \forall t\in\left[0,\,T\right]$

$\Leftrightarrow\quad x_S(t)y_{S'}(t)-t\,\dot{x}_O y_{S'}(t)=x_{S'}(t)y_S(t)-t\,\dot{x}_O y_S(t)\qquad \forall t\in\left[0,\,T\right]\qquad$ (6)

### *VII.1.a Proof of RESULT 1 and RESULT 2*

In this part, the source $S'$ is in CT motion:

$\exists\, x'_C$, $y'_C$, $\rho'_C\,(>0)$, $\omega'$ and $\varphi'$ such that $\begin{bmatrix}x_{S'}(t)\\ y_{S'}(t)\end{bmatrix}=\begin{bmatrix}x'_C\\ y'_C\end{bmatrix}+\rho'_C\begin{bmatrix}\sin(\omega' t+\varphi')\\ \cos(\omega' t+\varphi')\end{bmatrix}$.

We recall that for $S$, we also have $\begin{bmatrix}x_S(t)\\ y_S(t)\end{bmatrix}=\begin{bmatrix}x_C\\ y_C\end{bmatrix}+\rho_C\begin{bmatrix}\sin(\omega t+\varphi)\\ \cos(\omega t+\varphi)\end{bmatrix}$.

So (6) is equivalent to

$$\begin{aligned}&\left[\rho_C\sin(\omega t+\varphi)+x_C\right]\left[\rho'_C\cos(\omega' t+\varphi')+y'_C\right]-t\dot{x}_O\left[\rho'_C\cos(\omega' t+\varphi')+y'_C\right]\\&=\left[\rho'_C\sin(\omega' t+\varphi')+x'_C\right]\left[\rho_C\cos(\omega t+\varphi)+y_C\right]-t\dot{x}_O\left[\rho_C\cos(\omega t+\varphi)+y_C\right]\end{aligned}$$

$$\begin{aligned}&\Leftrightarrow\ \rho_C\,\rho'_C\sin\left[(\omega-\omega')t+\varphi-\varphi'\right]+\rho y'_C\sin(\omega t+\varphi)\\&+\rho'_C\,x_C\cos(\omega' t+\varphi')-\rho'_C\,y_C\sin(\omega' t+\varphi')\\&-\rho_C x'_C\cos(\omega t+\varphi)+x_C y'_C-x'_C\,y_C\\&=t\,\dot{x}_O\left[\rho'_C\cos(\omega' t+\varphi')-\rho_C\cos(\omega t+\varphi)\right]+t\dot{x}_O\left(y'_C-y_C\right)\end{aligned}$$

This equality stands for $\forall t\in\left[0,\,T\right]$.

For convenience, we call the first member of the last equality $G(t)$:

$$G(t) = \rho_C \rho'_C \sin[(\omega - \omega')t + \varphi - \varphi'] + \rho_C y'_C \sin(\omega t + \varphi)$$
$$+ \rho'_C x_C \cos(\omega' t + \varphi') - \rho'_C y_C \sin(\omega' t + \varphi') \qquad (7)$$
$$- \rho_C x'_C \cos(\omega t + \varphi) + x_C y'_C - x'_C y_C$$

And the second term $H(t)$:

$$H(t) = t\dot{x}_O[\rho'_C \cos(\omega' t + \varphi') - \rho_C \cos(\omega t + \varphi)] + t\dot{x}_O(y'_C - y_C) \qquad (8)$$

The functions $t \mapsto G(t)$ and $t \mapsto H(t)$ being analytic on $]0, T[$ , they are equal everywhere following the proposition. Hence $\frac{G(t)}{t} = \frac{H(t)}{t}$, $\forall t > 0$. Since $|G(t)|$ is bounded, we have: $\frac{G(t)}{t} \to 0$ when $t \to \infty$. Hence $\frac{H(t)}{t} \to 0$. But $\frac{H(t)}{t} = \dot{x}_O[\rho'_C \cos(\omega' t + \varphi') - \rho_C \cos(\omega t + \varphi)] + \dot{x}_O(y'_C - y_C)$. Convergence is possible if and only if $\dot{x}_O[\rho'_C \cos(\omega' t + \varphi') - \rho_C \cos(\omega t + \varphi)] + \dot{x}_O(y'_C - y_C) = 0$ *i.e.* $H(t) = 0, \ \forall t > 0$.

As a consequence, $G(t) = 0$.

The equality $H(t) = 0$ is satisfied

- if $\dot{x}_O \neq 0$, which implies $[\rho'_C \cos(\omega' t + \varphi') - \rho_C \cos(\omega t + \varphi)] + (y'_C - y_C) = 0$ (the observer is not stationary - case A- ),
- or if $\dot{x}_O = 0$ (the observer is stationary - case B - ).

1) case A (non stationary observer)

$$\left[\rho'_C\cos(\omega' t+\varphi')-\rho_C\cos(\omega t+\varphi)\right]+(y'_C-y_C)=0\Rightarrow\begin{cases}\rho'_C\cos(\omega' t+\varphi')-\rho_C\cos(\omega t+\varphi)=0\\ y'_C-y_C=0\end{cases}$$

We start by exploiting the first equality:

$$\rho'_C\cos(\omega' t+\varphi')-\rho_C\cos(\omega t+\varphi)=0\Rightarrow\begin{cases}\rho_C=\rho'_C=0\\ \text{or } \rho_C=\rho'_C\neq 0 \text{ and } \omega' t+\varphi'=-\omega t-\varphi\\ \text{or } \rho_C=\rho'_C\neq 0 \text{ and } \omega' t+\varphi'=\omega t+\varphi\end{cases}$$

Let us consider three cases:

- The case $\rho_C=\rho'_C=0$ must be discarded.
- $\rho_C=\rho'_C\neq 0$ and $\omega' t+\varphi'=-\omega t-\varphi$

  Now, let us exploit the equality $G(t)=0,\ \forall\ t$:

  $$G(t)=\rho_C^2\sin[2\omega t+2\varphi]+\rho_C y_C\sin(\omega t+\varphi)+\rho_C x_C\cos(\omega t+\varphi)+\rho_C y_C\sin(\omega t+\varphi)$$
  $$-\rho_C x'_C\cos(\omega t+\varphi)+x_C y_C-x'_C y_C$$

  $$=\rho_C^2\sin[2\omega t+2\varphi]+2\rho_C y_C\sin(\omega t+\varphi)+\rho_C(x_C-x'_C)\cos(\omega t+\varphi)+(x_C-x'_C)y_C$$

  The equality $G(t)=0,\ \forall\ t$ is incompatible with $\rho_C\neq 0$. This case must be discarded.

- $\rho_C=\rho'_C\neq 0$ and $\omega' t+\varphi'=\omega t+\varphi$

  Now, let us exploit the equality $G(t)=0,\ \forall\ t$:

  $$G(t)=\rho_C(x_C-x'_C)\cos(\omega t+\varphi)+(x_C-x'_C)y_C$$

  $G(t)=0$ implies that $x_C=x'_C$.

  Finally, $\begin{pmatrix}x_S(t)\\ y_S(t)\end{pmatrix}=\begin{pmatrix}x_{S'}(t)\\ y_{S'}(t)\end{pmatrix}$.

2) Case B (the observer is motionless):

We start by developing $G(t)$:

$$\begin{aligned} G(t) &= \rho_C\,\rho'_C\cos(\varphi-\varphi')\sin[(\omega-\omega')t]+\rho_C\,\rho'_C\sin(\varphi-\varphi')\cos[(\omega-\omega')t] \\ &+\rho_C(x'_C\sin\varphi+y'_C\cos\varphi)\sin\omega t+\rho_C(-x'_C\cos\varphi+y'_C\sin\varphi)\cos\omega t \\ &-\rho'_C(x_C\sin\varphi'+y_C\cos\varphi')\sin\omega' t+\rho'_C(x_C\cos\varphi'-y_C\sin\varphi')\cos\omega' t \\ &+x_C y'_C-x'_C y_C \\ &=0,\ \forall t \end{aligned}$$

Again, we have to consider two sub-cases:

- $\omega\neq\omega'$

  Because the functions $\sin[(\omega-\omega')t]$, $\cos[(\omega-\omega')t]$, $\sin\omega t$, $\cos\omega t$, $\sin\omega' t$ and $\cos\omega' t$ are analytic, all their coefficients are equal to zero, in particular those of $\sin[(\omega-\omega')t]$ and of $\cos[(\omega-\omega')t]$:

  $$\begin{cases}\rho_C\,\rho'_C\cos(\varphi-\varphi')=0\\ \rho_C\,\rho'_C\sin(\varphi-\varphi')=0\end{cases}$$

  which implies that $\rho_C=0$ or $\rho'_C=0$, which is in contradiction to the fact that $\rho_C>0$ and $\rho'_C>0$.

  Hence this sub-case must be discarded.

- $\omega=\omega'$

  In this case, $G(t)$ becomes

$$G(t) = \rho_C\, \rho'_C \sin(\varphi - \varphi') + \left[\rho_C \left(x'_C \sin\varphi + y'_C \cos\varphi\right) - \rho'_C \left(x_C \sin\varphi' + y_C \cos\varphi'\right)\right]\sin\omega t$$
$$+ \left[\rho_C \left(-x'_C \cos\varphi + y'_C \sin\varphi\right) + \rho'_C \left(x_C \cos\varphi' - y_C \sin\varphi'\right)\right]\cos\omega t$$
$$+ x_C y'_C - x'_C\, y_C .$$

$$G(t) = 0,\ \forall t \Rightarrow \begin{cases} \rho_C\, \rho'_C \sin(\varphi - \varphi') + x_C y'_C - x'_C\, y_C = 0 \\ \rho_C \left(x'_C \sin\varphi + y'_C \cos\varphi\right) - \rho'_C \left(x_C \sin\varphi' + y_C \cos\varphi'\right) = 0 \\ \rho_C \left(-x'_C \cos\varphi + y'_C \sin\varphi\right) + \rho'_C \left(x_C \cos\varphi' - y_C \sin\varphi'\right) = 0 \end{cases}$$

Let us denote by $\left[R_C \quad \theta_C\right]^T$ and $\left[R'_C \quad \theta'_C\right]^T$ the respective polar coordinates of $P_C = \begin{bmatrix} x_C \\ y_C \end{bmatrix}$ and $P'_C = \begin{bmatrix} x'_C \\ y'_C \end{bmatrix}$.

The last two equations are equivalent to

$$\begin{cases} \rho_C\, R'_C \cos(\varphi - \theta'_C) = \rho'_C\, R_C \cos(\varphi' - \theta_C) \\ \rho_C\, R'_C \sin(\varphi - \theta'_C) = \rho'_C\, R_C \sin(\varphi' - \theta_C) \end{cases}$$

hence equivalent to $\begin{cases} \rho_C\, R'_C = \rho'_C\, R_C \\ \varphi - \theta'_C = \varphi' - \theta_C \end{cases}$ or $\begin{cases} \rho_C\, R'_C = \rho'_C\, R_C \\ \varphi - \varphi' = \theta'_C - \theta_C \end{cases}$

We define now the positive constant $\mu = \dfrac{\rho'_C}{\rho_C} = \dfrac{R'_C}{R_C}$.

We inject this double equality in the first equation:

$$\rho_C\, \rho'_C \sin(\varphi - \varphi') + R_C\, R'_C \sin(\theta_C - \theta'_C) = 0$$
$$\Leftrightarrow \mu\left(\rho_C^2 - R_C^2\right)\sin(\varphi - \varphi') = 0$$

This equality is satisfied iff $\sin(\varphi - \varphi') = 0$ or $\rho_C = R_C$.

a) Let us exploit the nullity of $\sin(\varphi - \varphi')$:

Again, we have to consider two sub-sub-cases:

- $\varphi' = \varphi$

  In this case, $\theta'_C = \theta_C$ and as a consequence, $\begin{cases} x'_C = \mu\, x_C \\ y'_C = \mu\, y_C \end{cases}$.

The source $S'$ whose motion is defined by

$$\begin{bmatrix} x_{S'}(t) \\ y_{S'}(t) \end{bmatrix} = \mu \begin{bmatrix} x_C \\ y_C \end{bmatrix} + \mu\rho_C \begin{bmatrix} \sin(\omega t + \varphi) \\ \cos(\omega t + \varphi) \end{bmatrix} \quad (9)$$

is detected in the same bearings than $S$ during $[0, T]$.

See equation

- $\varphi' = \varphi + \pi$

In this case, $\theta'_C = \theta_C + \pi$ and, as a consequence, $\begin{cases} x'_C = -\mu x_C \\ y'_C = -\mu y_C \end{cases}$

$$\begin{bmatrix} x_{S'}(t) \\ y_{S'}(t) \end{bmatrix} = -\mu \begin{bmatrix} x_C \\ y_C \end{bmatrix} + \mu\rho_C \begin{bmatrix} \sin(\omega t + \varphi + \pi) \\ \cos(\omega t + \varphi + \pi) \end{bmatrix}$$
$$= -\mu \begin{bmatrix} x_C \\ y_C \end{bmatrix} - \mu\rho_C \begin{bmatrix} \sin(\omega t + \varphi) \\ \cos(\omega t + \varphi) \end{bmatrix}$$

which means that the source $S'$ is detected in the opposite bearings.

Hence this sub-sub-case must be discarded.

b) Now, let us exploit the equality $\rho_C = R_C$.

We deduce immediately that $\rho'_C = R'_C$

Hence the observer is in the circles in which $S$ and $S'$ are travelling.

The motion of $S$ and $S'$ are then given respectively by

$$\begin{bmatrix} x_S(t) \\ y_S(t) \end{bmatrix} = R_C \begin{bmatrix} \sin\theta_C + \sin(\omega t + \varphi) \\ \cos\theta_C + \cos(\omega t + \varphi) \end{bmatrix} \text{ and } \begin{bmatrix} x_{S'}(t) \\ y_{S'}(t) \end{bmatrix} = R'_C \begin{bmatrix} \sin\theta'_C + \sin(\omega t + \varphi') \\ \cos\theta'_C + \cos(\omega t + \varphi') \end{bmatrix}$$

or equivalently,

$$\begin{bmatrix} x_S(t) \\ y_S(t) \end{bmatrix} = 2R_C \begin{bmatrix} \sin\left(\frac{\omega t+\varphi+\theta_C}{2}\right)\cos\left(\frac{\omega t+\varphi-\theta_C}{2}\right) \\ \cos\left(\frac{\omega t+\varphi+\theta_C}{2}\right)\cos\left(\frac{\omega t+\varphi-\theta_C}{2}\right) \end{bmatrix} = 2R_C \cos\left(\frac{\omega t+\varphi-\theta_C}{2}\right) \begin{bmatrix} \sin\left(\frac{\omega t+\varphi+\theta_C}{2}\right) \\ \cos\left(\frac{\omega t+\varphi+\theta_C}{2}\right) \end{bmatrix}$$

and, using the same formula

and $\begin{bmatrix} x_{S'}(t) \\ y_{S'}(t) \end{bmatrix} = 2R'_C \cos\left(\frac{\omega t+\varphi'-\theta'_C}{2}\right) \begin{bmatrix} \sin\left(\frac{\omega t+\varphi'+\theta'_C}{2}\right) \\ \cos\left(\frac{\omega t+\varphi'+\theta'_C}{2}\right) \end{bmatrix}$

Since $\varphi-\theta'_C=\varphi'-\theta_C$, we got

$$\begin{bmatrix} x_{S'}(t) \\ y_{S'}(t) \end{bmatrix} = 2R'_C \cos\left(\frac{\omega t+\varphi+\theta_C-2\theta'_C}{2}\right) \begin{bmatrix} \sin\left(\frac{\omega t+\varphi+\theta_C}{2}\right) \\ \cos\left(\frac{\omega t+\varphi+\theta_C}{2}\right) \end{bmatrix}$$

As a consequence, the sources $S$ and $S'$ will be detected in the same bearings if and only if the sign of $\cos\left(\frac{\omega t+\varphi-\theta_C}{2}\right)$ and the sign of $\cos\left(\frac{\omega t+\varphi+\theta_C-2\theta'_C}{2}\right)$ are the same. Because the source never meets the observer, $\cos\left(\frac{\omega t+\varphi-\theta_C}{2}\right)$ is either positive or negative.

(i) When $\cos\left(\frac{\omega t+\varphi-\theta_C}{2}\right)>0$, then $-\frac{\pi}{2}<\frac{\omega t+\varphi+\theta_C-2\theta'_C}{2}<\frac{\pi}{2}$ which is equivalent to $\frac{\omega t+\varphi+\theta_C-\pi}{2}<\theta'_C<\frac{\omega t+\varphi+\theta_C+\pi}{2}$ $\quad \forall\ t\in[0,\ T]$.

In this case, $\theta(t)=\frac{\omega t+\varphi+\theta_C}{2}$.

This implies that

$$\underset{t \in [0,\ T]}{Sup}\left\{\frac{\omega t+\varphi+\theta_C-\pi}{2}\right\} < \theta'_C < \underset{t \in [0,\ T]}{Inf}\left\{\frac{\omega t+\varphi+\theta_C+\pi}{2}\right\}.$$

If $\omega > 0$, this double inequality is equivalent to

$$\frac{\omega T+\varphi-\theta_C-\pi}{2} < \theta'_C-\theta_C < \frac{\varphi-\theta_C+\pi}{2},$$

$$\Leftrightarrow \quad \theta(T)-\theta_C-\frac{\pi}{2} < \theta'_C-\theta_C < \theta(0)-\theta_C+\frac{\pi}{2}$$

If $\omega < 0$, it is equivalent to $\theta(0)-\theta_C-\frac{\pi}{2} < \theta'_C-\theta_C < \theta(T)-\theta_C+\frac{\pi}{2}$.

(ii) When $\cos\left(\frac{\omega t+\varphi-\theta_C}{2}\right) < 0$, then $\theta(t)=\frac{\omega t+\varphi+\theta_C}{2}+\pi$.

Similar calculations yields the same constraints:

If $\omega > 0$, then $\theta(T)-\theta_C-\frac{\pi}{2} < \theta'_C-\theta_C < \theta(0)-\theta_C+\frac{\pi}{2}$,

If $\omega < 0$, then $\theta(0)-\theta_C-\frac{\pi}{2} < \theta'_C-\theta_C < \theta(T)-\theta_C+\frac{\pi}{2}$.

### *VII.1.bProof of RESULT 3 (distinguishability between CT and CV motion)*

Let the source $S'$ in CV motion:

$$\exists\ x_{S'}(0),\ y_{S'}(0),\ \dot{x}_{S'} \text{ and } \dot{y}_{S'} \text{ such that } \begin{bmatrix} x_{S'}(t) \\ y_{S'}(t) \end{bmatrix} = \begin{bmatrix} x_{S'}(0) \\ y_{S'}(0) \end{bmatrix} + t \begin{bmatrix} \dot{x}_{S'} \\ \dot{y}_{S'} \end{bmatrix}.$$

$$(5) \Leftrightarrow \left[x_C+\rho_C \sin(\omega t+\varphi)-t\dot{x}_O\right]\left(y_{S'}(0)+t\,\dot{y}_{S'}\right)=\left[x_{S'}(0)+t\left(\dot{x}_{S'}-\dot{x}_O\right)\right]\left[y_C+\rho_C\cos(\omega t+\varphi)\right],\ \forall\ t$$

$$\Leftrightarrow x_C y_{S'}(0)+t\left(x_C \dot{y}_{S'}-\dot{x}_O y_{S'}(0)\right)+\rho_C\, y_{S'}(0)\sin(\omega t+\varphi)+t\,\rho_C\,\dot{y}_{S'}\sin(\omega t+\varphi)-t^2\dot{x}_O\dot{y}_{S'}$$
$$=x_{S'}(0)y_C+x_{S'}(0)\rho_C\cos(\omega t+\varphi)+t\left(\dot{x}_{S'}-\dot{x}_O\right)y_C+t\;\rho_C\left(\dot{x}_{S'}-\dot{x}_O\right)\cos(\omega t+\varphi),\;\forall\, t$$

which can be re-arranged as follows

$$x_C y_{S'}(0)-x_{S'}(0)y_C+t\left(x_C\dot{y}_{S'}-\dot{x}_{S'}y_C-\dot{x}_O y_{S'}(0)+\dot{x}_O y_C\right)-t^2\dot{x}_O\dot{y}_{S'}$$
$$=\rho_C\left[x_{S'}(0)\cos(\omega t+\varphi)-y_{S'}(0)\sin(\omega t+\varphi)-t\,\dot{y}_{S'}\sin(\omega t+\varphi)+t\left(\dot{x}_{S'}-\dot{x}_O\right)\cos(\omega t+\varphi)\right],\;\forall\, t$$

This equality between a polynomial in $t$ and a function of sine and cosine is impossible. Hence, there is no source in CV motion that can be seen in the same bearing as $S$ during $[0,\, T\,]$.

### VII.2 Proof RESULT 5 (observability in FB-CTTMA)

Again, for the sake of simplicity, we consider the observer located at the origin. So, the observer position at any time $\forall t \in [\,0,\, T\,]$ is:

$$\begin{bmatrix} x_O(t) \\ y_O(t) \end{bmatrix}=\begin{bmatrix} 0 \\ 0 \end{bmatrix},\ \forall t \in [\,0,\, T\,]$$

.

Let two sources $S$ (the one of interest) and $S'$ another source in CT motion *i.e.*

$$\begin{bmatrix} x_S(t) \\ y_S(t) \end{bmatrix}=\begin{bmatrix} x_C \\ y_C \end{bmatrix}+\rho_C\begin{bmatrix} \sin(\omega t+\varphi) \\ \cos(\omega t+\varphi) \end{bmatrix}\ \text{and}\ \begin{bmatrix} x_{S'}(t) \\ y_{S'}(t) \end{bmatrix}=\begin{bmatrix} x'_C \\ y'_C \end{bmatrix}+\rho'_C\begin{bmatrix} \sin(\omega' t+\varphi') \\ \cos(\omega' t+\varphi') \end{bmatrix}$$

detected in the same bearings and emitting a pure tone $f_0$ and $f_0'$.

Under these hypotheses, the common received noise-free frequency for the sources $S$ and $S'$ is

$$f(t) = f_0\left[1 - \dot{R}(t)/C\right] = f_0'\left[1 - \dot{R}'(t)/C\right] \qquad (10)$$

Since the observer is motionless, the radial speed is

- for $S$, $\dot{R}(t) = \dot{x}_S(t)\sin\theta(t) + \dot{y}_S(t)\cos\theta(t)$
- and for $S'$, $\dot{R}'(t) = \dot{x}_{S'}(t)\sin\theta(t) + \dot{y}_{S'}(t)\cos\theta(t)$.

On the other hand, we have,

- $\dot{x}_S(t) = \rho_C\omega\cos(\omega t + \varphi)$ and $\dot{y}_S(t) = -\rho_C\omega\sin(\omega t + \varphi)$
- $\dot{x}_{S'}(t) = \rho_C'\omega'\cos(\omega' t + \varphi')$ and $\dot{y}_{S'}(t) = -\rho_C'\omega'\sin(\omega' t + \varphi')$.

We know from RESULT 2 that for some homothetic ratio $\mu$, we have $\rho'_C = \mu\rho_C$.

The turn rates and initial angles are respectively equal: $\omega' = \omega,\ \varphi' = \varphi + \alpha$ where $\alpha = 0$ or $\alpha = \theta_C - \theta_C'$.

Hence $\dot{x}_{S'}(t) = \mu\rho_C\omega\cos(\omega t + \varphi + \alpha)$ and $\dot{y}_{S'}(t) = -\mu\rho_C\omega\sin(\omega t + \varphi + \alpha)$. We deduce that

$$\begin{cases} \dot{R}(t) = \rho_C\omega\sin(\theta(t) - \omega t - \varphi) \\ \dot{R}'(t) = \mu\rho_C\omega\sin(\theta(t) - \omega t - \varphi - \alpha) \end{cases}$$

Eq. (10) is equivalent to

$$f_0\left[1 - \frac{\rho_C\,\omega}{C}\sin\left[\theta(t) - \omega t - \varphi\right]\right] = f_0'\left[1 - \frac{\mu\rho_C\,\omega}{C}\sin\left[\theta(t) - \omega t - \varphi - \alpha\right]\right]$$

Hence, $f_0 = f_0'$ and $\sin\left[\theta(t) - \omega t - \varphi\right] = \mu\sin\left[\theta(t) - \omega t - \varphi - \alpha\right]$.

As a consequence, $\alpha = 0$ and $\mu = 1$.

The source $S'$ is identical to $S$.

## VII.3 Proof of RESULT 6 (MFB-CTTMA).

### *VII.3.a Expression of the FIM in a block structure for the FB-CTTMA*

The Fisher information matrix (FIM) about $Y$ takes the following form:

$$F\left(Y\middle|\,\theta_m,\,f_m\right)=\sum_{k=1}^{N}\frac{1}{\sigma_\theta^2\left(t_k\right)}\nabla_Y\theta\left(Z,t_k\right)\nabla_Y^T\theta\left(Z,t_k\right)+\sum_{k=1}^{N}\frac{1}{\sigma_f^2\left(t_k\right)}\nabla_Y f\left(Y,t_k\right)\nabla_Y^T f\left(Y,t_k\right) \qquad (11)$$

Due to the special structure of the state vector (2), the FIM (11) can be partitioned into four blocks:

$$F\left(Y\middle|\,\theta_m,\,f_m\right)=\left[\begin{array}{c|c}\gamma_0 & c_0^T\\ \hline c_0 & F\left(Z\middle|\theta_m\right)+F\left(Z\middle|\,f_m\right)\end{array}\right] \qquad (12)$$

with:

- $F\left(Z\middle|\,\theta_m\right)=\sum_{k=1}^{N}\frac{1}{\sigma_\theta^2\left(t_k\right)}\nabla_Z\theta\left(Z,t_k\right)\nabla_Z^T\theta\left(Z,t_k\right)$, which is the usual FIM about the state vector $Z$ when only the bearings are measured;
- $F\left(Z\middle|\,f_m\right)=\sum_{k=1}^{N}\frac{1}{\sigma_f^2\left(t_k\right)}\nabla_Z f\left(Y,\,t_k\right)\nabla_Z^T f\left(Y,\,t_k\right)$ (13), which is the FIM about $Z$ given the frequency measurements is the following $\left(5\times5\right)$ matrix;

- The block $c_0$ of (12) is a vector $\left(5\times1\right)$:

$$c_0=\sum_{k=1}^{N}\frac{1}{\sigma_f^2\left(t_k\right)}\left[\frac{\partial f\left(Y,\,t_k\right)}{\partial f_0}\right]\nabla_Z f\left(Y,\,t_k\right), \qquad (14)$$

- and $\gamma_0$ is a scalar: $\gamma_0=\sum_{k=1}^{N}\frac{1}{\sigma_f^2\left(t_k\right)}\left[\frac{\partial f\left(Y,\,t_k\right)}{\partial f_0}\right]^2$ (15)

We are going to exploit the structure of $F\left(Y\middle|\theta_m, f_m\right)$ to prove a useful property about the accuracy of the TMA when the number of received frequencies increases.

### *VII.3.bExpression of the FIM in a block structure for the MFB-CTTMA*

As previously (see (12)), the FIM of MFB-CTTMA can be partitioned as:

$$F\left(Y\middle|\theta_m, f_{0,m},\cdots, f_{P-1,m}\right)=\left[\begin{array}{ccc|c} \gamma_0 & 0 & 0 & c_0^T \\ 0 & \ddots & 0 & \vdots \\ 0 & 0 & \gamma_{P-1} & c_{P-1}^T \\ \hline c_0 & \cdots & c_{P-1} & F\left(Z|\theta_m\right)+F\left(Z\middle|f_{0,m}\right)+\cdots+F\left(Z\middle|f_{P-1,m}\right) \end{array}\right]$$

The vectors $c_p$ and the scalars $\gamma_p$ are similarly defined (14) and $\gamma_0$ (15) respectively.

We are interested by the inverse of the submatrix $F\left(Z|\theta_m\right)+F\left(Z\middle|f_{0,m}\right)+\cdots+F\left(Z\middle|f_{P-1,m}\right)$ corresponding to the position and the velocity of the source.

We are going to use the following classic result of linear algebra (see [29]):

Lemma:

*Consider a non-singular matrix* $A=\left[\begin{array}{c|c} A_{11}(p\times p) & A_{12}(p\times q) \\ \hline A_{21}(q\times p) & A_{22}(q\times q) \end{array}\right]$ *and*

$A^{-1}=\left[\begin{array}{c|c} B_{11}(p\times p) & B_{12}(p\times q) \\ \hline B_{21}(q\times p) & B_{22}(q\times q) \end{array}\right]$ *its inverse, both partitioned in four blocks.*

*Then* $B_{22}^{-1}=A_{22}-A_{21}A_{11}^{-1}A_{12}$, *provided* $A_{11}$ *is non-singular.*

We then identify $A_{11}$ to $\begin{bmatrix}\gamma_0 & 0 & 0\\ 0 & \ddots & 0\\ 0 & 0 & \gamma_{P-1}\end{bmatrix}$, $A_{22}$ to

$F(Z|\theta_m)+F(Z|f_{0,m})+\cdots+F(Z|f_{P-1,m})$, $A_{12}$ to $\begin{bmatrix}c_0^T\\ \vdots\\ c_{P-1}^T\end{bmatrix}$ and $A_{21}$ to $\begin{bmatrix}c_0 & \cdots & c_{P-1}\end{bmatrix}$.

Because the bearing rate is not equal to zero, the frequency rate is non-null too and as a consequence the matrix $A_{11}$ is nonsingular. The lemma can be applied as follows:

We get $B_{22}=B(Z|\theta_m, f_{0,m},\cdots, f_{P-1,m})$ given by

$$B(Z|\theta_m, f_{0,m},\cdots, f_{P-1,m})^{-1}=F(Z|\theta_m)+F(Z|f_{0,m})+\cdots+F(Z|f_{P-1,m})-\begin{bmatrix}c_0 & \cdots & c_{P-1}\end{bmatrix}\begin{bmatrix}\gamma_0 & 0 & 0\\ 0 & \ddots & 0\\ 0 & 0 & \gamma_{P-1}\end{bmatrix}^{-1}\begin{bmatrix}c_0^T\\ \vdots\\ c_{P-1}^T\end{bmatrix}.$$

We show readily that

$$\begin{bmatrix} c_0 & \cdots & c_{P-1} \end{bmatrix} \begin{bmatrix} \gamma_0 & 0 & 0 \\ 0 & \ddots & 0 \\ 0 & 0 & \gamma_{P-1} \end{bmatrix}^{-1} \begin{bmatrix} c_0^T \\ \vdots \\ c_{P-1}^T \end{bmatrix} = \sum_{p=0}^{P-1} \gamma_p^{-1} c_p c_p^T .$$

As a consequence, we get

$$B\left(Z\middle|\theta_m, f_{0,m}, \cdots, f_{P-1,m}\right)^{-1} = F\left(Z\middle|\theta_m\right) + F\left(Z\middle| f_{0,m}\right) + \cdots + F\left(Z\middle| f_{P-1,m}\right) - \sum_{p=0}^{P-1} \gamma_p^{-1} c_p c_p^T . \qquad (16)$$

This first result will help us to prove the property of the BMF-TMA in the coming section.

### *VII.3.c Proof of RESULT 6*

Now we are able to prove the double inequality.

$$B\left(Z\middle|\theta_m, f_{0,m}, \cdots, f_{P-2,m}, f_{P-1,m}\right) \preceq B\left(Z\middle|\theta_m, f_{0,m}, \cdots, f_{P-2,m}\right) \preceq \cdots \preceq B\left(Z\middle|\theta_m, f_{0,m}\right) \preceq B\left(Z\middle|\theta_m\right).$$

- Left inequality: $B\left(Z\middle|\theta_m, f_{0,m}, \cdots, f_{P-2,m}, f_{P-1,m}\right) \preceq B\left(Z\middle|\theta_m, f_{0,m}, \cdots, f_{P-2,m}\right)$ .

  We can re-write (16) as follows

  $$B\left(Z\middle|\theta_m, f_{0,m}, \cdots, f_{P-2,m}, f_{P-1,m}\right)^{-1} = B\left(Z\middle|\theta_m, f_{0,m}, \cdots, f_{P-2,m}\right)^{-1} + F\left(Z\middle| f_{P-1,m}\right) - \gamma_{P-1}^{-1} c_{P-1} c_{P-1}^T$$

  It turns out that the matrix $F\left(Z\middle| f_{P-1,m}\right) - \gamma_{P-1}^{-1} c_{P-1} c_{P-1}^T$ is positive semidefinite

  since the matrix $\left[\begin{array}{c|c} \gamma_{P-1} & c_{P-1}^T \\ \hline c_{P-1} & F\left(Z\middle| f_{P-1,m}\right) \end{array}\right]$ is the Fisher information matrix

  $F\left(Y\middle| f_{P-1,m}\right)$, if we acquire $f_{P-1,m}$ only.

  Hence $B\left(Z\middle|\theta_m, f_{0,m}, \cdots, f_{P-2,m}, f_{P-1,m}\right)^{-1} - B\left(Z\middle|\theta_m, f_{0,m}, \cdots, f_{P-2,m}\right)^{-1}$ is positive semidefinite.

- Right inequality: $B\left(Z\middle|\theta_m, f_{0,m}\right) \preceq B\left(Z\middle|\theta_m\right)$

  We consider the matrix $F\left(Y\middle|\,\theta_m, f_m\right)=\left[\begin{array}{c|c}\gamma_0 & c_0^T \\ \hline c_0 & F\left(Z\middle|\theta_m\right)+F\left(Z\middle|\,f_m\right)\end{array}\right]$ and carry out the lemma again, with $A_{11}=\gamma_0$, $A_{22}=F\left(Z\middle|\theta_m\right)+F\left(Z\middle|\,f_m\right)$, $A_{12}=c_0^T$ and $A_{21}=c_0$.

  We get readily

  $B\left(Z\middle|\theta_m, f_m\right)^{-1}=F\left(Z\middle|\theta_m\right)+F\left(Z\middle|\,f_m\right)-\gamma_0^{-1}c_0c_0^T$.

  For the same reason as previously, we have

  $F\left(Z\middle|\theta_m\right)+F\left(Z\middle|\,f_m\right)-\gamma_0^{-1}c_0c_0^T \succeq F\left(Z\middle|\theta_m\right)$,

  hence

  $B\left(Z\middle|\theta_m, f_m\right) \preceq B\left(Z\middle|\theta_m\right)$.

  This inequality has a meaning if the observer is not motionless (observable case). Otherwise, $B\left(Z\middle|\theta_m\right)$ does not exist and by extension, the inequality remains valid.

  This completes the proof of (4).

# VIII References

[1] Rong Li, X. and Jilkov, V.P.

*Survey of Maneuvering Target Tracking. Part I: Dynamic Models*.

IEEE Transactions on Aerospace and Electronic Systems, **39**, 4 (2003), 1333-1364.

[2] Kolb, R.C., Hollister, F.H..

*Bearings-Only Target Motion Estimation*.

In Proceedings of the 1st Asilomar Conference on Circuits Systems, Nov.1967.

[3] Bucy, R.S. and Sene, K.D.

*Digital synthesis of non-linear filters*.

Automatica, Vol.7 (1971), 287-298.

[4] Nardone, S.C., Lindgren, A.G. and Gong, K.F.

*Fundamental Properties and Performance of Conventional Bearings-Only Target Motion Analysis*.

IEEE Transactions on Automatic Control, **29**, 9 (1984), 775-787.

[5] Nardone, S.C. and Aidala, V.J.

*Observability Criteria for Bearings-Only Target Motion Analysis*.

IEEE Transactions on Aerospace and Electronic Systems, **17**, 2 (1981), 162-166.

[6] Fogel, E. and Gavish, M.

*N th-order dynamics target observability from angle measurements.*

IEEE Transactions on Aerospace and Electronic Systems, **24**, 3 (1988), 305-308.

[7] Payne, A.N.

*Observability conditions for angle-only tracking*.

Proceedings of the 22th Asilomar Conference on Signals, Systems and Computers, Nov. 1988.

[8] Jauffret, C. and Pillon, D.

*Observability in Passive Target Motion Analysis*.

IEEE Transactions on Aerospace and Electronic Systems, **32**, 4 (1996), 1290-1300.

[9] Becker,K.

*A General Approach to TMA Observability from Angle and Frequency Measurements.*

IEEE Transactions on Aerospace and Electronic Systems, **32**, 1 (1996), 487-494

[10] Koteswara Rao, S.

*Algorithm for Detection of Manoeuvring Targets in Bearings-Only Passive Target Tracking.*

*IEE Proceedings of Radar Sonar and Navigation.,* **146**, 3 (1999), 141-146.

[11] Farina, A.

*Target Tracking with Bearings-Only Measurements*.

Signal Processing, **78**, (1999) 61-78.

[12] Jauffret, C., Pillon, D. and Pignol, A.C.

*Bearings-Only Maneuvering Target Motion Analysis from a Nonmaneuvering Platform*.

IEEE Transactions on Aerospace and Electronic Systems, **46**, 4 (2010), 1934-1948.

[13] Sanjeev Arulampalam, M., Ristic, M., Gordon, N. and Mansell, T.

*Bearings-Only Tracking of Manoeuvring Targets Using Particle Filters*.

EURASIP Journal on Applied Signal Processing, **15** (2004), 2351-2365.

[14] Ristic, B. and Sanjeev Arulampalam, M.

*Tracking a Manoeuvring Target Using Angle-Only Measurements: Algorithms and Performance.*

Signal Processing, **83** (2003) 1223-1238

[15] Clavard, J., Pillon, D., Pignol, A.C. and Jauffret, C.

*Bearings-Only Target Motion Analysis of a Source in a Circular Constant Speed Motion from a Non-Maneuvering Platform*.

In Proceedings of the 14th International Conference on Information Fusion, Chicago, 5-8 Jul. 2011.

[16] Laplace, P.S.

*Mémoire sur la détermination des orbites des comètes*.

Mémoires de l'Académie Royale des Sciences de Paris, 1780.

[17] Gauss, K.F.

*Theoria Motus: Theory of the motion of the heavenly bodies moving about the sun in conic sections*.

Boston: Little Brown, 1857.

[18] Sorenson, H.W.

*Least-Squares Estimation: from Gauss to Kalman.*

IEEE Spectrum, **7**, (1970), 63-68.

[19] Sabol, C., Carter, S. and Vallado D.

*A Fresh Look at Angles-Only Orbit Determination.*

AAS/AIAA Astrodynamics Specialist Conference, Girdwood (Alaska), August 1999.

[20] Li, Q., Guo, F.C., Zhou, Y. and Jiang W.

*Observability of Satellite to Satellite Passive Tracking from Angle Measurements*.

IEEE International Conference on Control and Automation, ICCA-2007, Guangzhou, May 30 to 1 June 2007.

[21] Li, Q., Guo, F.C., Li, J. and Zhou, Y.

*Research of Satellite-to-Satellite Passive Tracking Using Bearings-Only Measurements.*

*In J2000 ECI Frame*, IEEE International conference on Radar 2006, ICR-2006, Shanghai, Oct. 2006, 16-19.

[22] Passerieux, J.M., Pillon, D., Blanc-Benon, P. and Jauffret, C.

*Target Motion Analysis with Bearings and Frequencies Measurements via Instrumental Variable Estimator*.

IEEE International Conference on Acoustics, Speech and Signal Processing, Glasgow (GB), ICASSP-89, 23-26 May 1989, 2645-2648.

[23] Jauffret, C., Blanc-Benon, P. and Pillon*, D.*

*Multi Frequencies And Bearing Target Motion Analysis : Properties and Sonar Applications*.

In Proceedings of the 11th International Conference on Information Fusion, Cologne, 1-3 Jul. 2008.

[24] Dufour, F. and Mariton, M.

*Tracking a 3D Maneuvering Target with Passive Sensors*.

IEEE Transactions on Aerospace and Electronic Systems, **27**, 4 (1991), 725-739.

[25] Zhan, R. and Wan, J.

*Passive Maneuvering target tracking using 3D constant-turn model*.

Proc. IEEE Conf. On Radar, Verona, New York, USA, 24-27 April 2006, 404-4011.

[26] Trevrrow M.V., Vasiliev B. and Vagle S.

*Directionality and maneuvering effects on a surface ship underwater acoustic signature.*

JASA, **124**, 2 (2008), 767-778.

[27] Spiegel, M.R.

*Schaum's Outline Series : Complex Variables* (1968).

[28] Dennis Jr., J. E.

*A User's Guide to Nonlinear Optimization Algorithms*.

Proceedings of IEEE, **72**, 12 (1984), 1765-1776.

[29] Frank Ayres, JR.

*Schaum's Outline Series : Theory and Problems of Matrices* (1962), 55-57.

Julien Clavard was born in Ploemeur, France, in 1985. He received the master degree “signal et trajectographie” from the Université du Sud Toulon-Var (USTV), France, in 2009. He is currently pursuing a Ph.D. degree in engineer sciences; his work is about Target Motion Analysis methods for passive sonar systems.

Denis Pillon, comes from a small French mountain called "Le Jura". He received the Diplôme d’Ingénieur from Ecole Supérieure de Physique et de Chimie Industrielle (ESPCI-Paris) in 1977 and the Diplôme d’Etudes Approfondies in probability theory from the Jussieu University, Paris in 1977. From 1978 to 1979 he worked in the area of operational research at the Centre InterArmées de Recherche Opérationnelle (CIRO) agency of the ministère de la Défense. Since 1980 he has been employed by Thomson Compagny (now Thales Compagny), France. From 1980 to 1981 he worked on sonar array processing. From 1982 to 1986, he was consultant at the GERDSM for which he worked on sea trial analysis and TMA. From 1987 to 1989, he worked on tracking and track clustering and in 1990 he was appointed group leader of signal and data processing laboratory at Thomson Sintra company, Sophia Antipolis,

France. From 1992 to 1999, he was consultant at the DCN sonar laboratory. He worked on new sonar arrays and various submarine combat systems. Since 2000, he has been sonar expert at Thales Underwater Systems (Sophia-Antipolis). His current researches are about passive sonar performances estimation, submarine and torpedo array processing, and long term prospective studies for submarine warfare.

Annie-Claude Pignol born in France on November 10, 1965, received the Diplôme d'Etudes Appronfondies in Optics and Image Processing from the Université de Toulon et du Var, Toulon, France, in 1988 and the title of « Docteur de l'Université » in 1991 from the Université de Toulon et du Var, France.

Since Sept. 1994, she has been at the Université de Toulon et du Var where she teaches electronic systems. Her researches were focused signal processing applied to biomedical systems before turning them to Target Motion Analysis.

Claude Jauffret born in France on March 29, 1957, received the diplôme d'Etudes Appronfondies in Applied Mathematics from Saint Charles University, Marseille, France, in 1981, the Diplôme d'Ingénieur from Ecole Nationale Supérieure d'Informatique et de Mathématiques Appliqués de Grenoble, Grenoble, France, in 1983, the title of « Docteur de l'Université » in 1993 and the « Habilitation à Diriger des Recherches » from the Université de Toulon et du Var, France.

From Nov. 1983 to Nov. 1988, he worked on passive sonar systems, more precisely on target motion analysis at GERDSM, France. After a sabbatical year at the University of Connecticut (from Nov. 1988 to Dec. 1989) during which he worked of tracking problems in cluttered environment, he developed researches in tracking, data fusion, and extraction in CERDSM. Since Sept. 1996, he has been at the Université de Toulon et du Var where he teaches statistical signal processing. His current researches are about observability, estimation in non linear systems as they appear in tracking problems.